4
Characteristics and Properties of Microporous Structures

I. ADSORPTION AND DESORPTION IN MICROPOROUS MEDIA

A. Microporous Adsorbent from the Synthesis to the Uses

Most existing processes for synthesis of microporous adsorbents comprise, as the final stage, a treatment of the obtained porous materials under high temperatures. When the synthesis is achieved, the fresh micropores are not empty but contain some gas or vapor–gas mixture consisting of volatile components delivered from the solid phase during the synthesis and/or products of their oxidation. When the adsorbent is cooled, the micropores adsorb also the gas from the environment (probably air):

$$\mathrm{Ads} + \mathrm{G} \rightarrow \mathrm{Ads} \cdot \mathrm{G} \tag{4.1}$$

When the adsorbent is, after all, in contact with the gas, adsorption of which is needed, the interaction between the gas and the adsorbent consists not in the entering of the gas into voids inside the adsorbent but in the replacement of the previously adsorbed volatile components with the new adsorbate:

$$\mathrm{Ads} \cdot \mathrm{G} + \mathrm{G}^* \rightarrow \mathrm{Ads} \cdot \mathrm{G}^* + \mathrm{G} \tag{4.2}$$

The kinetics of reaction (4.2) is given by the following equation:

$$\frac{dC_{\mathrm{AdsG}}}{dt} = k_{-\mathrm{GG}^*} C_{\mathrm{AdsG}^*} P_{\mathrm{G}} - k_{+\mathrm{GG}^*} C_{\mathrm{AdsG}} P_{\mathrm{G}^*} \tag{4.3}$$

where k_{+GG^*} and k_{-GG^*} are constants of the rate of the direct and the reverse reactions (4.2), C_i is the concentration of ith component in the solid phase, and P_j is the partial pressure of jth volatile component in the gaseous phase.

Now, let us consider some options in the technique of adsorption performance:

1. The experiment is carried out in a closed box, and the delivered component G remains in the system; then the adsorption process continues until the equilibrium:

$$k_{-GG^*} C_{AdsG^*} P_G = k_{+GG^*} C_{AdsG} P_{G*} \tag{4.4}$$

   while the measured weight of the adsorbate brings the wrong information about the adsorptive properties of the initial adsorbent. If the adsorptive characteristics of G and G* are comparable and the molecular weight of G is equal or more than that of G* ($m_G \geq m_{G^*}$), the researcher measures even "negative adsorption."
2. The experiment is carried out by injecting gas G* into the adsorbent carrier, while the gaseous products are removed away. Then, $P_G \approx 0$, and the solution of Eq. (4.3) is

$$\begin{aligned} C_{AdsG} &= C_{(AdsG)0} \exp(-k_{+GG*} P_{G*} t) \\ &= C_{(AdsG)0} \exp(-k_{+GG*} t) \end{aligned} \tag{4.5}$$

   where $C_{(AdsG)0}$ is the initial concentration of the adsorbent carrying the initial adsorbate. Then the resulting adsorbate consists only of AdsG*, but the loss in the weight of G should be taken into account.
3. Operations described above by item 2 are preceded by removal of G: before injecting G*, the adsorbent is heated on purpose to remove G as it is possible then cooled in vacuum. Then the resulting concentration of G is minor—but still not zero.
4. The cycle "heating adsorbent with removal of adsorbate, cooling in vacuum, and injecting G*" is repeated several times, then the measured change of the weight is

$$\delta W_{AdsG^*} \approx \rho_{Ads} \nu_{Ads} [C_{AdsG^*}(T) - C_{AdsG^*}(T_0)] \tag{4.6}$$

   where ν_{Ads} is the amount of the adsorbent, ρ_{Ads} is its density, T_0 is the temperature to which the adsorbent is heated before being

cooled, and T is the temperature under which G* is injected. If w_n is the value of $\delta W_{\mathrm{AdsG}^*}$ after n^{th} iteration, the condition of the correctness of the performance of the measurements is given by the following equation:

$$w_n = w_{n-1} \pm \delta w \tag{4.7}$$

where δw is the error of the measurements of the weight.

Unfortunately, as it was noted in Chapter 2, condition (4.7) for micropores can never be satisfied because of hysteresis, therefore, the correct organization of the measurements of adsorption is extremely complicated.

As an additional option, one might suggest the isolation of the adsorbent immediately after the achievement of its synthesis, but also such technique does not allow avoiding errors.

In several situations, for example, when the adsorbent is used for gas separation, it can be sufficient to measure the composition of the gas phase, first of all P_{G^*}.

In the further analysis of adsorption phenomena, we will assume that the experimental measurements are organized enough correctly and all errors are related only to hysteresis phenomena, as that was described in Chapter 2.

B. Reversible Adsorption and Desorption

The reversibility of the performance of adsorption–desorption processes means that

The processes are carried out very slowly, and the current partial pressure of G* in Eq. (4.2) differs a little only from that over the adsorbent (i.e., for adsorption it is a little *more* and for desorption, a little *less*).

The temperature is controlled (probably specified), and the only factor influencing the change of the weight of the product is the adsorption–desorption of G*, due to the different (while almost equal) pressures of G* just over the adsorbent and far above.

C. Fundamental Physical Causes of Adsorption

The main driving force for adsorption is the reduction of free energy of pores accumulated on the stage of pore formation. Adsorption process is always exothermal and always accompanied by the reduction of the entropy of the system "pore + adsorbate." In any solid or liquid, the particles at the surface are subject to unbalanced forces of attraction normal to the

surface plane (if applicable). In discusses about the fundamentals of adsorption, it may be useful in several cases to distinguish between physical adsorption involving only relatively weak intermolecular forces (due to the free energy of pores, especially micropores) and chemisorption involving essentially the formation of a chemical bond between the adsorbate molecule and the surface of the adsorbent (simply said, a chemical reaction between the pore wall and adsorbate molecules). For chemisorption, the reduction of the pore free energy is not the only driving force: the second driving force is the heat effect of the chemical reaction of chemisorption.

Although the above distinction is conceptually useful, many real cases are intermediate between two those options, and it is not always possible to categorize a particular system unequivocally [1,2].

Physical adsorption can be distinguished from chemisorption according to one or more of the following criteria:

Physisorption does not involve the sharing or transfer of electrons, which always maintains the "individuality" (meaning no chemical changes) of the interacting species. The interactions are well reversible (except for micropores), enabling desorption to occur at the same temperature, although the process may be limited by the diffusion factor. Chemisorption involves chemical bonding and is definitely irreversible even in macropores.

Physisorption is not as specific as chemisorption: physically adsorbed molecules may move inside the pores, whereas chemically adsorbed molecules are immobilized at pore walls.

The absolute-value heat effect (the change of enthalpy in the sorption process) for physisorption is (except for micropores) much shorter than for chemisorption.

Hysteresis effects for adsorption–desorption cycle are observed for physisorption/only in micro- and mesopores/and for chemisorption (always, independent of the adsorbing structure).

In principle, chemisorption is typical for situations when the chemical reaction between the pore wall material and the adsorbate molecules is possible in normal conditions, without any regard to internal surface in the solid reagent. A very specific situation is found when the process of adsorption is accompanied by a chemical reaction, in which the adsorbate experiences chemical transformation without visible changes for the adsorbent (heterogeneous catalysis). As it was notified in Chapters 1 and 2, micropores allow reactions that would be just impossible in other conditions. In the case of heterogeneous catalysis, the driving force of the process is initially the reduction of the free energy of pores, but then it is the reduction of the chemical potential of the entire system, while the products

do not usually remain inside the pores but leave them. Thus, heterogeneous catalysis can be considered as a very specific and complex form of chemisorption in micropores.

The divergence between these two mechanisms of adsorption is illustrated by Table 4.1.

As follows from Table 4.1, physisorption in micropores has intermediate features between physisorption in macropores on plate surface and chemisorption.

Physisorption in nonpolar solids is normally attributed to forces of interactions between the solid surface and the adsorbate molecules. Those forces are similar to the van der Waals forces (attraction–repulsion) between molecules. The forces of attraction involving electrons and nuclei of all components of the system have electrostatic origin and are termed *dispersion forces*. These exist in all kinds of matter, independently on its interior structure. The nature of the dispersion forces was first recognized in the 1930s by London.

The dipole–dipole interaction energy (for attraction—negative, of course) can be estimated from the following equation [2]:

$$E_D = -\frac{\text{Const}_{\text{DD}}}{\text{Dis}^6} \tag{4.8}$$

where E_D is the dispersion energy, Const_{DD} is a constant of dipole–dipole attraction, and Dis is the distance between the interacting particles.

In addition to dipole–dipole interaction, other possible dispersion interactions contributing physisorption include dipole–quadrupole and quadrupole–quadrupole interactions. If these are incuded into the expression for the interaction energy, it is written as follows:

$$E_D = -\frac{\text{Const}_{\text{DD}}}{\text{Dis}^6} - \frac{\text{Const}_{\text{DQ}}}{\text{Dis}^8} - \frac{\text{Const}_{\text{QQ}}}{\text{Dis}^{10}} \tag{4.9}$$

where Const_{DQ} and Const_{QQ} are constants of dipole–quadrupole and quadrupole–quadrupole interactions, respectively. Quadrupole interactions involve symmetrical molecules with atoms of different electronegativity like CO_2. The quadrupole moment of such molecules leads to their interactions with polar surfaces. Taking into account that the contribution of dipole–quadrupole and quadrupole–quadrupole interactions decreases fast with the distance, the decisive role is, in most situations, of dipole–dipole interaction, and dipole–quadrupole and quadrupole–quadrupole interactions can be neglected.

TABLE 4.1 Comparison of Physisorption to Chemisorption

Factor of comparison	Physisorption in macropores and plate surface	Physisorption in micropores	Chemisorption	Heterogeneous catalysis in micropores
Driving force for the adsorption process	Reduction of free energy of pores	Reduction of free energy of pores	Both chemical reaction and reduction of free energy of pores	First reduction of free energy of pores, then the chemical reaction
Reversibility	Reversible	Problematic reversibility	Irreversible	Irreversible
Absolute value of heat effect (kJ/mol)	<20	<80	<400	No limit
Motion of adsorbed molecules	Easily possible	Constrained	Impossible	Constrained
Hysteresis of adsorption–desorption	Negligible	Moderate	Strong	Strong

When an adsorbate molecule approaches close to a solid surface enough to allow interpenetration of the electron clouds, the repulsion factor arises; its contribution can be represented semiempirically by the following expression:

$$E_R = \frac{\text{Const}_\text{R}}{\text{Dis}^{12}} \tag{4.10}$$

where E_R is the repulsion energy (positive value, of course!) and Const_R is a constant of repulsion. Thus, the total potential energy of van der Waals interactions comprises two terms: dipole–dipole attraction (if dipole–quadrupole and quadrupole–quadrupole interactions are neglected) and repulsion:

$$E_\sum = -\frac{\text{Const}_\text{DD}}{\text{Dis}^6} + \frac{\text{Const}_R}{\text{Dis}^{12}} \tag{4.11}$$

D. The Polanyi Theory of Adsorption Potential

Among numerous theories of pore–adsorbate interaction considered in Ref. 3, we notice first of all the Polanyi theory of adsorption potential. This theory became the methodological base for volume-filling micropore theory (VFMT) largely employed in the adsorption science.

According to Polanyi, a quantification of the adsorption potential is required. It is defined as the amount of work needed for moving a molecule from a pore to infinity. The adsorption space (pore volume) is assumed to be composed of many equipotential adsorption energy surfaces varying from a maximum in the finest pores to zero in the bulk solution. Hence, for a given adsorbent, the equipotential surface should be the same for all adsorbates. Consequently, a plot of adsorbate volume vs. adsorption potential should result in a single characteristic curve applicable to all adsorbates on that particular adsorbent. Thus, this theory suggests that an adsorption isotherm could be predicted for any compound or any adsorbent for which a characteristic adsorption curve has been obtained [2].

In addition to adsorption isotherms, the adsorption equilibrium relationships are the isostere and the isobar. The isostere is, in general, a plot of the $\ln P$ vs. $1/T$ at a constant amount of vapor adsorbed. The slope of the isostere corresponds to the heat of adsorption [2].

E. Classification of Adsorption Isotherms

The majority of physisorption isotherms may be grouped into six types. In most situations, at sufficiently low surface coverage, the isotherm reduces to

a linear form often compared to Henry's law region. If adsorbent is heterogeneous, this linear region may fall below the lowest experimentally measurable pressure. The principal types of isotherms are presented on Figs. 4.1–4.6.

The reversible type 1 isotherm (Langmuir isotherm) is concave to the argument P/P_0 axis and approaches a limiting value as $P/P_0 \to 1$. For micropores, the curve has a very sharp rising at the low pressure. Isotherms of such type are usual for homogeneous microporous solids, external surfaces of which are negligible (e.g., active carbon or molecular sieves). For such adsorbents, the adsorption process is determined mostly by the microporous substructure, and other factors can be neglected [2].

Langmuir isotherm is the most important for adsorption science but not alone. Among other curve types, very important is multilayer adsorption isotherm curve (Fig. 4.2).

The reversible type 2 isotherm is the normal form of isotherm obtained for nonporous or microporous adsorbent and represents unrestricted mono-multilayer adsorption. The beginning of the quasilinear middle section of the isotherm corresponds the monolayer completed and the multilayer adsorption beginning [2].

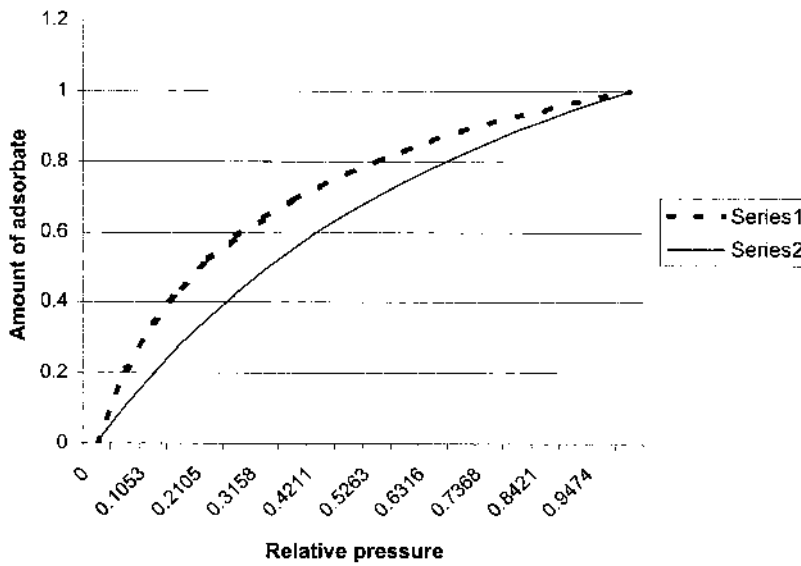

FIG. 4.1 Adsorption isotherm type 1 (Langmuir) for gas on homogeneous adsorbent. Series 1: microporous adsorbent; Series 2: external surface.

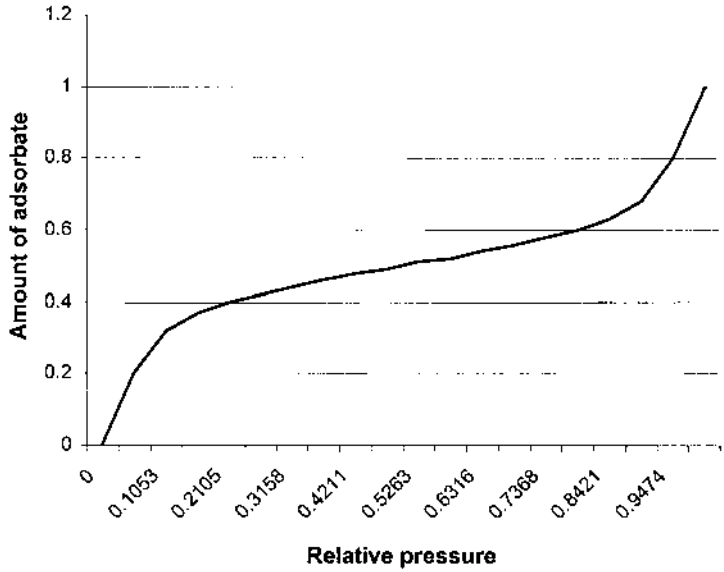

FIG. 4.2 Adsorption isotherm type 2 (BET) on homogeneous adsorbent.

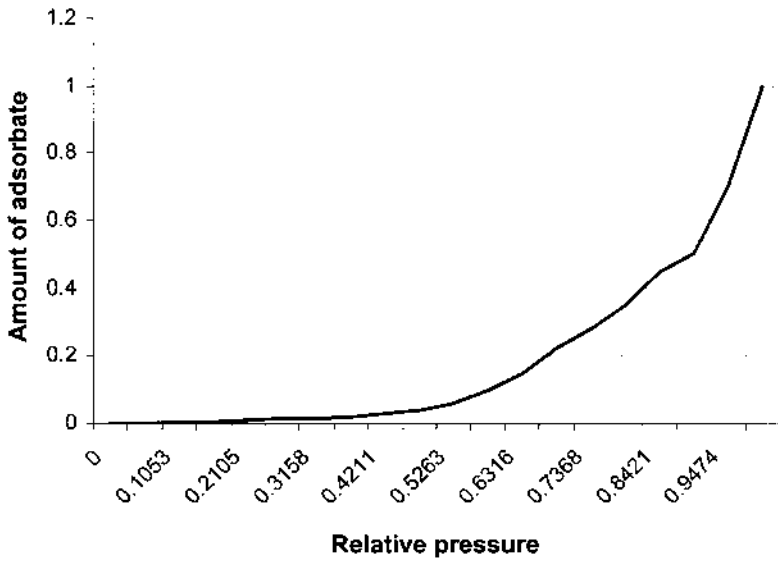

FIG. 4.3 Type 3 of adsorption isotherm curves.

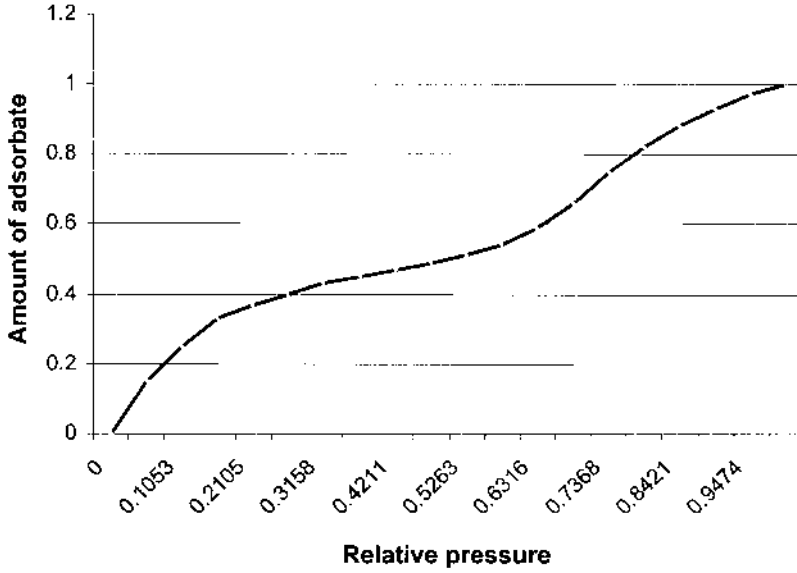

FIG. 4.4 Adsorption isotherm curve–type 4.

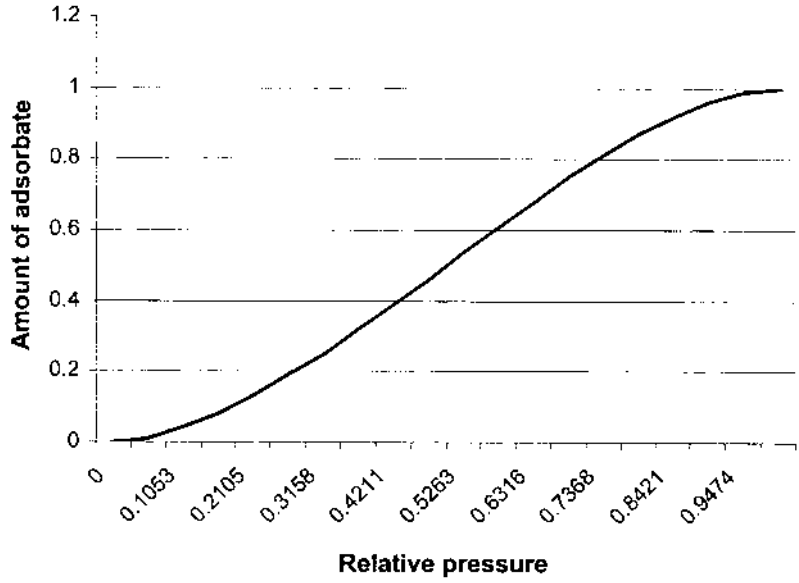

FIG. 4.5 Isotherms of adsorption: type 5.

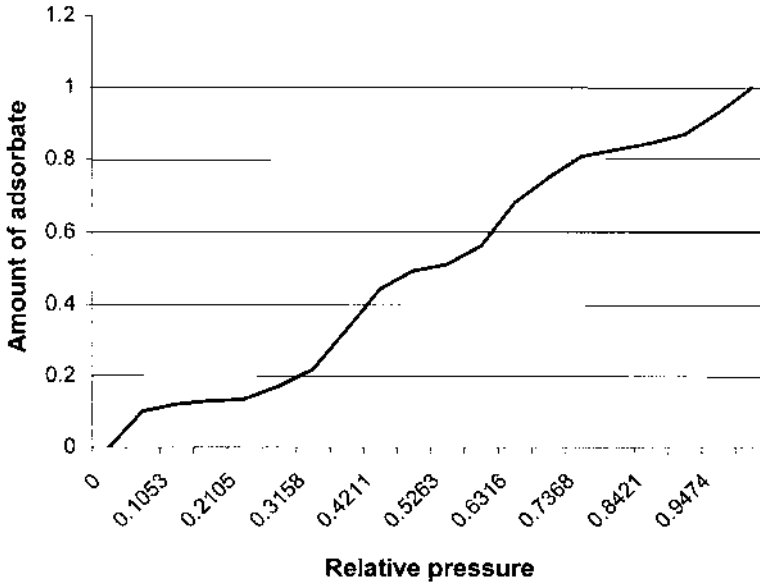

FIG. 4.6 Type 6 of adsorption isotherms.

Types 1 and 2 are found in condition that the adsorbate is compatible with the material of pore walls. Otherwise, under low pressures the amount of adsorbate is low (see Fig. 4.3).

The reversible type 3 isotherm is typical for such a specific situation we considered in Chapters 1 and 2: adsorption of vapors (e.g., water vapor) on hydrophobic adsorbents like active carbon. When $P/P_0 \rightarrow 1$, the vapor condensation in the micropores starts.

In the case when the adsorbate is compatible with the pore wall material, another form is obtained (see Fig. 4.4).

According to Ref. 2, the type 4 isotherms are irreversible and correspond to hysteresis loops described in Chapter 2. The form of these isotherms is usually attributed to capillary condensation in the mesopores. The limiting uptake for such isotherms is $P/P_0 \gg 1$. Other possible explanations for such effects include destruction of some pores because of rising pressure and, as result, increase of the internal volume or chemisortion-related effects. This form of adsorption isotherms is obtained for many of mesoporous industrial adsorbents, comprising silica and alumina gels adsorbing water [2–4].

The form of adsorbent isotherm curve for weak interactions adsorbent–adsorbate is given on Fig. 4.5.

According to Ref. 2, the type 5 isotherm is related to the type 3 isotherm in a specific situation when the adsorbent–adsorbate interaction is weak [2].

And the last example in this series: multilayer adsorption in micropores (see Fig. 4.6).

The type 6 isotherm represents stepwise multilayer adsorption on a uniform nonporous surface. The step height represents the monolayer capacity for each adsorbed layer and, in the simplest case, remains approximately constant for two or more adsorbed layers. Such curves are obtained with some noble gases on graphitized carbon blacks under temperatures of liquid nitrogen [2].

F. Models of Adsorption in Equilibrium

1. Henry's Law

The simplest adsorption isotherm, in which the amount adsorbed varies directly with the gas pressure, is very similar to Henry's law:

$$Q_{\text{ads}} = K_{\text{ads}} C_e \tag{4.12}$$

where Q_{ads} is the amount of the adsorbate, K_{ads} is the isotherm constant, and C_e is the equilibrium concentration in the fluid volume. Isotherms by Eq. (4.12) are typical for situations when the amount of the fluid over the adsorbent is much less than the adsorptive capacity of the adsorbent and the adsorbed layer is extremely diluted [2,5].

2. Freundlich Isotherm

The equilibrium relationships in adsorption are sometimes described by a Freundlich relationship. This is valid for adsorptive processes with no change in the configuration of the molecules in the adsorbed state. Freundlich isotherm has the following form:

$$Q_{\text{ads}} = K_{\text{ads}} (C_e)^{1/n_{fr}} \tag{4.13}$$

where n_{fr} is an empiric constant depending on the nature of the adsorbent and the adsorbate. Freundlich isotherm seems valid for adsorption on heterogeneous surfaces described by the discrete model (see Chapter 3), each class of cells obeying the Langmuir equation (see below). According to Freundlich isotherm, the amount adsorbed increases infinitely with the increase of the concentration or the partial pressure of the fluid to adsorb. Of course, such isotherm is not sufficient when coverage becomes enough high. At low concentrations, Freundlich isotherm does not reduce to the

linear isotherm. Thus, Freundlich isotherm represents experimental results for moderate concentrations of the fluid to adsorb [2].

3. Langmuir Isotherm

This is applicable first of all to macroporous adsorbents, also to some microporous materials. This isotherm is applicable to both physisorption and chemisorption and derived under the following assumptions:

The adsorbed gas behaves ideally in the gas phase.
The adsorbate forms a monomolecular layer only.
The adsorptive surface is homogeneous.
Interactions between adsorbate molecules are negligible.
The motion of adsorbate molecules around the surface is impossible or negligible.

In accordance to the above assumptions, the equilibrium between the gas and the solid phases is described by the following equation [compare to Eq. (4.1)]:

$$\mathrm{Ads} + \mathrm{G} \Longleftrightarrow \mathrm{Ads} \cdot \mathrm{G} \tag{4.14}$$

Equation (4.14) leads to the condition of equilibrium:

$$K_{\mathrm{ads}} = \frac{C_{\mathrm{AdsG}}}{C_{\mathrm{Ads}} C_{\mathrm{G}}} = \frac{Q_{\mathrm{AdsG}}}{Q_{\mathrm{Ads}} C_{\mathrm{G}}} \tag{4.15}$$

where C_i is the concentration of ith component in equilibrium and Q_i is the amount of ith component in the solid phase.

The condition of the balance of the adsorbate is given by the following equation:

$$Q_{\mathrm{Ads}} + Q_{\mathrm{AdsG}} = Q_{\mathrm{Ads},0} \tag{4.16}$$

where $Q_{\mathrm{Ads},0}$ is the initial amount of the adsorbate. Equations (4.15) and (4.16) bring

$$Q_{\mathrm{AdsG}} = \frac{C_{\mathrm{G}} K_{\mathrm{ads}} Q_{\mathrm{Ads},0}}{K_{\mathrm{ads}} C_{\mathrm{G}} + 1} \tag{4.17a}$$

Or

$$\theta_{\mathrm{AdsG}} = \frac{C_{\mathrm{G}} K_{\mathrm{ads}}}{K_{\mathrm{ads}} C_{\mathrm{G}} + 1} \tag{4.17b}$$

where $\theta_{AdsG} = Q_{AdsG}/Q_{Ads,0}$ and the graphical representation of Eq. (4.17a) is exactly Fig. 4.1. When $C_G \to \infty$, $Q_{AdsG} \to Q_{Ads,0}$. For low values of C_G, $Q_{AdsG} \approx C_G K_{ads} Q_{Ads,0}$ (Henry's law).

Langmuir isotherm is basic for the science of adsorption.

4. BET Equation

In 1938, Brunauer, Emmett, and Teller showed how to extend the Langmuir's approach to the multilayer adsorption, that is BET equation. The basic assumptions for BET are as follows:

Each molecule in the first adsorbed layer is considered to provide one site for the second and subsequent layers.

The molecules in the layers behave essentially as saturated liquid, and interactions between different layers do not depend on the interactions between the down layer and the adsorbent.

The above assumptions allow us to write the equations of reactions of multilayer formation:

$$Ads + G \Longleftrightarrow Ads \cdot G \tag{4.18a}$$

$$Ads \cdot G + G \Longleftrightarrow Ads \cdot G_2 \tag{4.18b}$$

$$Ads \cdot G_k + G \Longleftrightarrow Ads \cdot G_{k+1} \tag{4.18c}$$

Equations (4.18) correspond to the following equations for the condition of equilibrium:

$$K_{ads'} = \frac{C_{AdsG}}{C_{Ads} C_G} = \frac{Q_{AdsG}}{Q_{Ads} C_G} \tag{4.19a}$$

$$K_{ads''} = \frac{C_{AdsG2}}{C_{AdsG} C_G} = \frac{Q_{AdsG2}}{Q_{AdsG2} C_G} \tag{4.19b}$$

$$K_{ads} = \frac{C_{AdsG(k+1)}}{C_{AdsGk} C_G} = \frac{Q_{AdsG(k+1)}}{Q_{AdsGk} C_G} \tag{4.19c}$$

As for Langmuir isotherm, Eqs. (4.19) with the balance condition (4.16) are transformed to

$$\frac{Q_{AdsG} = C_G K_{ads} Q_{Ads,0}/K_{ads} C_G + 1 - C_G}{(1 - C_G)} \tag{4.20}$$

or

$$Q_{\mathrm{AdsG}} = (P/P_s)K_{\mathrm{ads}}Q_{\mathrm{Ads},0}/(K_{\mathrm{ads}}P/P_s + 1 - P/P_s)/(1 - P/P_s) \qquad (4.21)$$

where the physical sense of all terms is the same as in Eq. (4.17).

Let us notify that BET for low pressures is reduced to a Langmuir-like form.

G. Models of the Structure of Adsorbate

On the internal pore surface, an adsorbed molecule may hop along the surface when it attains sufficient activation energy and an adjacent adsorption site becomes available. Describing the porosity reduction in random structures, P. B. Vissher and J. E. Cates suggested a model for computing the motion of a solid–liquid interface by means of Lagrangian grid with constant-stress periodic boundary conditions [6].

H. Volume-Filling Micropore Theory

For micropores, derivations of adsorption isotherms need a comprehension about the internal structure of the adsorbent. The most widespread concept regarding this problem is volume-filling micropore theory [VFMT; sometimes also called *theory of volume-filling micropore* (TVFM)]. VFMT is based on the assumption that the adsorptive capacity of micropores is limited not by their surface but by their volume. As we noted in the previous chapters, this assumption is based on the recognized experimental data on properties of micropores. In this aspect, VFMT seems correct in principle. The adsorption is considered as the result of the adsorbate molecule entering a pore between the walls, as described according to the Polanyi concept above, regarding energetics of inside the empty space in solids. The accomplished work is proportional to $R_g T(\ln(P/P_s))$. A convenient starting point is the method of integral transforms, relating an overall isotherm θ_t to a local isotherm θ_l and the pore energy distribution [7]:

$$\theta_t(T, P) = \int_0^\infty \theta_l(T, P, \varepsilon)\chi_c(\varepsilon)\, d\varepsilon \qquad (4.22)$$

where $\chi_c(\varepsilon)$ gives a distribution of adsorption energies. If a variational technique called the *condensation approximation* (CA) is applied to the local isotherm, Eq. (4.22) is reduced to [7]

$$\theta_t(T, P) = \int_0^\infty \chi_c(\varepsilon)\, d\varepsilon \Longleftrightarrow \chi_c(\varepsilon) = -\frac{\partial \theta_t}{\partial \varepsilon} \qquad (4.23)$$

If θ_l is the Langmuir isotherm and gaussian pore-size distribution assumed, an overall isotherm is of the Dubinin–Radushkevich–Kaganer type [7]:

$$\theta_\Sigma = \mathrm{Exp}\left[-\mathrm{B_a}\frac{\mathrm{T}\ln(P/P_0)}{\beta_a}\right]^2 \tag{4.24}$$

$$\varepsilon = \varepsilon_0 - R_g T \ln(P/P_0) \tag{4.25}$$

where B_a is a semiempirical parameter depending on the adsorbent and β_a is the affinity coefficient according to CA.

Figure 4.7 below presents different profiles of adsorption isotherm curves obtained for different values of $b_a = B_a/\beta_a^2$.

As follows from Fig. 4.7, the choice of b_a is very important for the form of the resulting curve: Series 3 absolutely differs from Series 1! Let us also note that the resulting curve (especially its beginning at low pressures) does not always correspond to the Langmuir-like isotherm given by Fig. 4.1.

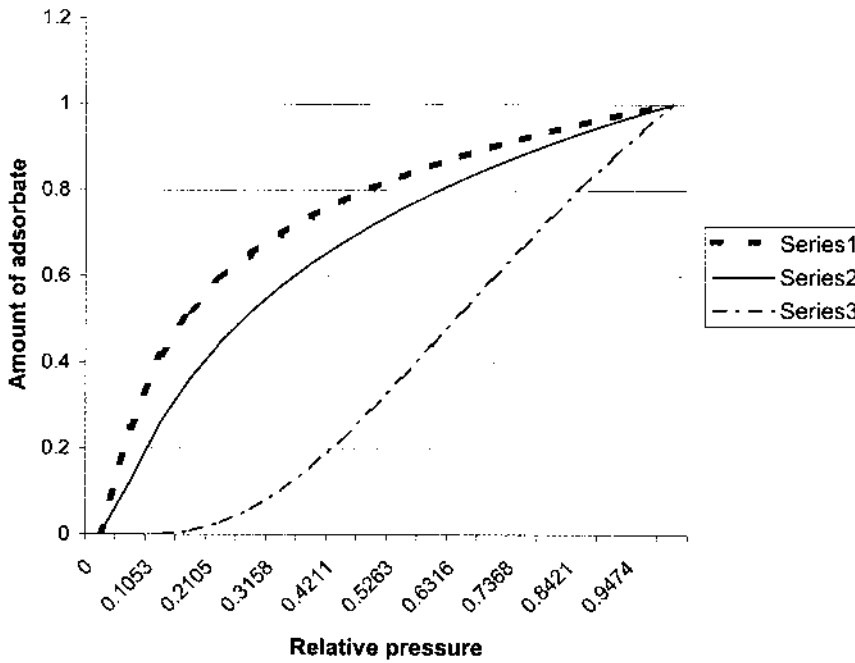

FIG. 4.7 Adsorption isotherm curves in VFMT: Series 1: $b_a = 1/(10R_gT)^2$; Series 2: $b_a = 1/10/(R_gT)^2$; Series 3: $b_a = 1/(R_gT)^2$.

Aiming to generalize VFMT, Dubinin and Astakhov replaced the gaussian distribution by "quasigaussian" and put forward a more general equation [8]:

$$\theta_\Sigma = \exp\left\{-B_a\left[\frac{T\ln(P/P_0)}{\beta_a}\right]^{n_e}\right\} \tag{4.26}$$

where n_e is an empirical parameter (in quasi–gaussian form, n_e is instead 2). For active carbons, n_e changes from 1 to 3 [8].

Aiming to apply VFMT to heterogeneous adsorbents, Stoeckli proposed a model taking into account their heterogeneity. Stoeckli assumed that a real adsorbent contains elements that can be separately described by the general equations of VFMT, but the semiempirical parameters change, depending on the adsorbent material. Stoeckli presented the solution for a heterogeneous material as the following integral [9–11]:

$$\theta_\Sigma = \int_0^\infty \theta_h(B_a)\exp(-B_a Y_\beta)\, dB_a \tag{4.27a}$$

where $\theta_h(B_a)$ is the local homogeneous solution for parameter B_a and

$$Y_\beta = \left(\frac{T\ \ln(P/P_0)}{\beta_a}\right)^2 \tag{4.27 b}$$

For particular solutions, θ_h is found from Eq. (4.22). Authors of VFMT pretend that Eq. (4.24) is applicable to all the possible homogeneous adsorbents.

McEnaney used VFMT for the estimation of sizes of micropores, based on the assumption that the decrease in the characteristic energy ε_0 in Eq. (4.25) is correlated with increases in micropore size determined by molecular probes Q_m, using an empirical equation [12]:

$$Q_m = 4.691\exp(-0.0666\varepsilon_0) \tag{4.28}$$

Stoeckli and Houriet showed that the parameters B_a and Q_{Ads0} change considerably for different active carbons [13].

VFMT was applied to description of the adsorption of vapors onto microporous adsorbents with both homogeneous and heterogeneous structures. One can take into account the association of the adsorbate molecules inside the pores for ordinary surfaces. The theoretical affinity

coefficient β_a can be calculated by different methods, comprising molar volume, molar parachor or electronic polarization [14].

It was shown that taking into account the factor of heterogeneity is indispensable in the case of strongly activated carbons [14].

VFMT was used also for the solution of kinetic problems, such as diffusivity-limited adsorption on micropores [14]. VFMT allowed researchers to find that the micropores could be treated as slots between the graphitic planes of the microcrystallites [14].

The relation between Dubinin–Radushkevich parameters and thermodynamic functions, especially the enthalpy of immersion, also was studied [14]. It was shown that the correlation exists at the limits of the estimated experimental error.

An attempt to relate the Dubinin–Radushkevich equation to BET was carried out by Tsunoda [15–17]: the author suggested that the pre-exponential coefficient B_a in Eq. (4.26) can be related with the BET parameter K_{ads} in a linear form:

$$B_a = -a_d \ln K_{\text{ads}} + b_d \tag{4.29}$$

where a_d and b_d are constant coefficients. Tsunoda suggested Eq. (4.29) for active carbons but did not mention what is the average dispersion of Eq. (4.29), particularly in comparison with the experimental error. The principal error of his suggestions seems to consist in establishing a formal correlation between BET (derived for surfaces) and Dubinin–Radushkevich equation designed for micropores. Such suggestion seems too doubtful without a serious theoretical research.

I. Analysis of Assumptions in VFMT

Now, following the previous review of VFMT, let us analyze the assumptions accepted in VFMT.

1. The main assumption in VFMT is the suggestion of adsorbate molecules reacting with pore volume—not pore wall, not pore surface, but the pore volume. This assumption correlates with all known experimental data about micropores, and there is no reason to make it in doubt.
2. The second assumption in VFMT is the condensation approximation given by Eq. (4.25). This assumption seems very problematic, because it is not clear how one takes into account the specificity of interactions between adsorbents and different gases and/or vapors. A pore, energy of which is found sufficient to adsorb fluids, is assumed to be filled entirely, without any intermediate

state. What about fluids having different compatibility with the pore wall material? This question stays without answer.

3. Another very problematic assumption in VFMT is suggestions about structural properties of adsorbents. These suggestions are not based on any analysis of structural characteristics determined by synthesis process, just some suppositions, and nothing more. Why gauss distribution of pores in size? Why the same distribution but in energy?
4. The fourth assumption in VFMT is more specific: Stoeckli's suggestion of Gibbs-like energy distribution of structural fragments in heterogeneous adsorbent. Though this assumption seems more logical and correlating with some of results obtained in Chapter 3, that contradicts the second assumption in VFMT (gauss distribution of micropores in size or energy). Though Stoeckli's suggestion seems more particular, that is very important, because most of industrial adsorbents are heterogeneous.

Thus, we have mentioned four principal assumptions in VFMT, among which three seem very doubtful. Is it possible to improve the logical structure of VFMT? This question is analyzed below.

J. Theory of Reversible Adsorption of Simple Gases by Micropore Volume (Langmuir-like Model)

Let us consider a very slow process of gas adsorption by a homogeneous microporous adsorbent, structural properties of which are determined by its preparation conditions and estimated by methods described in Chapter 3. Let us make the following assumptions about the pore–adsorbate interactions:

The process of micropore–gas interaction is close to equilibrium.
The adsorbed gas behaves ideally in the gas phase.
The adsorption in micropore is limited by pore volume only.
Interactions between adsorbate molecules are negligible.

These assumptions are very similar to those formulated for the derivation of Langmuir's isotherm.

In accordance to the above assumptions, the equilibrium between the gas G and the pore having the initial energy ε per unit of internal substance and containing adsorbate is described by the following equation [compare to Eq. (4.14)]:

$$\text{Pore}(\varepsilon) + \text{G} \longleftrightarrow \text{Pore}(\varepsilon) \cdot G \tag{4.30}$$

Equation (4.30) leads to the following condition of equilibrium:

$$K_{\text{ads}}(\varepsilon) = \frac{C_{\text{Pore}}(\varepsilon)_{\text{G}}}{C_{\text{Pore}}(\varepsilon)P_{\text{G}}} \tag{4.31}$$

where P_{G} is the partial pressure of G out pores, $C_{\text{Pore}}(\varepsilon)$ is the volume part of the pore still able to adsorb gas G, and $C_{\text{Pore}}(\varepsilon)_{\text{G}}$ is the volume part of the pore already occupied by the gas. The values $C_{\text{Pore}}(\varepsilon)_{\text{G}}$ and $C_{\text{Pore}}(\varepsilon)$ can be, in principle, found from the following equations:

$$C_{\text{Pore}}(\varepsilon) = 1 - \frac{\theta_{\text{G,c}}(\varepsilon)}{\theta_{\text{G, max}}(\varepsilon)} \tag{4.32}$$

$$C_{\text{Pore}}(\varepsilon)\text{G} = \frac{\theta_{\text{G,c}}(\varepsilon)}{\theta_{\text{G, max}}(\varepsilon)} \tag{4.33}$$

where $\theta_{\text{G,max}}(\varepsilon)$ is the maximal capacity of the micropore to adsorb the gas and $\theta_{\text{G,c}}(\varepsilon)$ is the current amount of G in the micropore. Since the adsorption process reduces the free energy of pores, the value of $K_{\text{ads}}(\varepsilon)$ increases exponentially with ε:

$$K_{\text{ads}}(\varepsilon) = K_{\text{ads}}(\varepsilon_0)\exp\frac{\gamma_{\text{p}}\varepsilon}{R_g T} \tag{4.34}$$

where $K_{\text{ads}}(\varepsilon_0)$ and γ_p are semiempirical parameters depending on both pore wall material and the adsorbate. Hence, the amount of the adsorbate in a micropore characterized by energy ε is found from Eq. (4.31):

$$\theta_{\text{Pore}}(\varepsilon)_{\text{G}} = \frac{K_{\text{ads}}(\varepsilon)P_{\text{G}}}{1 + K_{\text{ads}}(\varepsilon)P_{\text{G}}} \tag{4.35}$$

and the resulting equation for the adsorption isotherm is given by the following equation:

$$\theta_{\Sigma}(P_G) = \varsigma P_G \int_{\varepsilon_{\min}}^{\varepsilon_{\max}} \frac{f(\varepsilon)K_{\text{ads}}(\varepsilon)}{1 + K_{\text{ads}}(\varepsilon)P_G} d\varepsilon \tag{4.36}$$

where the sense of parameters ξ, $f(\varepsilon)$, and Q_0 is the same as in Chapter 3.

Now, let us analyze Eqs. (4.34)–(4.36).

1. Equations (4.34)–(4.36) contains two semiempirical parameters ($K_{\text{ads}}(\varepsilon_0)$ and γ_p) depending not only on the adsorbent but also the adsorbate and some parameters ($\varepsilon_{\min}$, $\varepsilon_{\max}$, etc.) related to the

adsorbent preparation conditions. Since preparation-related parameters can be evaluated from the synthesis conditions, as it was described in Chapter 3, Eqs. (4.34)–(4.36) should be considered as two-parametric (containing two fitted parameters).

2. When $P_G \to 0$, obviously $\theta_\Sigma(P_G) \to 0$.
3. When $P_G \to \infty$, $\theta_\Sigma(P_G) \to \text{CONST} \sim V_{\text{por}}$ (V_{por} is the total volume of micropores in the treated sample).

Figure 4.8 presents adsorption isotherm curves obtained on the base of eqs. (4.34)–(4.36) for different values of γ_p.

As follows from Fig. 4.8, also Langmuir-like approach brings curves very sensitive to the value of the exponential term, but this does not influence the form of the entire curve (compare to Fig. 4.7). This result demonstrates one advantage of the proposed model: sensitivity to the exponential term is quantitative but not qualitative.

It is interesting to compare the adsorption isotherm curves obtained by the different methods. Figure 4.9 presents the curves obtained in accordance to Dubinin's VFMT (Eqs. (4.22)–(4.25)), the above-presented Langmuir-like approach [Eqs. (4.34)–(4.36)], and an intermediate curve, building of

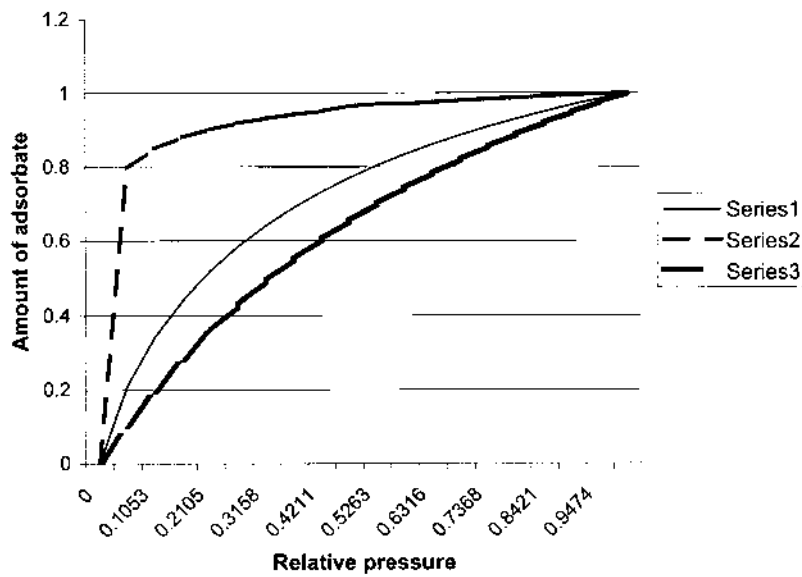

FIG. 4.8 Langmuir-like approach for micropores, adsorption isotherm curves: Series 1: $\gamma_p = 1$; Series 2: $\gamma_p = 10$; Series 3: $\gamma_p = 0.1$.

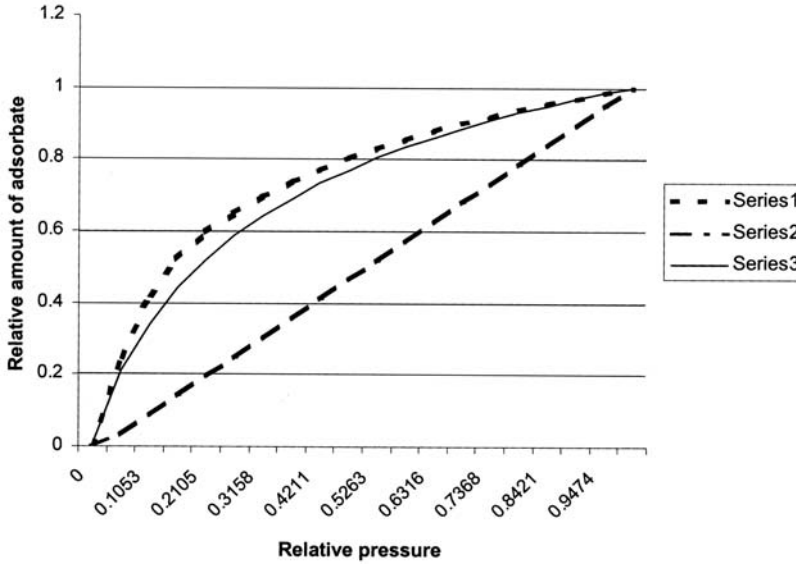

FIG. 4.9 Forms of Dubinin, Langmuir-like, and mixed (intermediary) adsorption isotherm curves: Series 1: Isotherm adsorption curve built according to VFMT; Series 2: Mixed (intermediary) curve built on the base of the combination of condensation approximation with Gibbs energy distribution; Series 3: Langmuir-like curve.

which combines condensation approximation from VFMT with Gibbs energy distribution.

As follows from Fig. 4.9, the intermediary solution (CA + Gibbs distribution) provides definitely wrong results. Both other curves are very similar. Hence, the main advantage of Langmuir-like building of the adsorption isotherm curve for micropores consists not in a "good" form but in the minimal number of empirical parameters to fit.

For homogeneous adsorbents, both models need two fitted parameters. However:

In VFMT, these are empirical parameters, physical sense of which is problematic and values of which can be found only from experiments, while in Langmuir-like model the fitted parameters are semiempirical and can be, in principle, found not only from experiments but also from quantum calculations.

For heterogeneous adsorbents, VFMT needs much more fitted parameters (from 4 to 6), they all are empirical, while the Langmuir-like model still needs two semiempirical parameters

(because the heterogeneous situation also is modeled by methods of thermodynamics of nonequilibrium [18]).

Equations (4.34)–(4.36) were applied by the author to experimental isotherms of adsorption obtained on very different adsorbents: active carbons prepared in steady state [14], active carbons prepared in non-steady state [19], and silica and alumina gels [20]. Structural parameters of the adsorbents were estimated in accordance with the recommendations presented in Chapter 3. The comparison of the experimental data with the theoretical curves allowed the following conclusions:

The general form of the theoretical curve found by Eqs. (4.34)–(4.36) is always quasi-Langmuir: very similar to the traditional Langmuir isotherm, but the rising at $P_G \to 0$ is much more sharp than in the traditional case.

The error (evaluated by least square method) was always very short — on the level of the experimental error.

It was very interesting to notice that the increase of the number of experimental points sometimes reduced the calculated error of theoretical curves, which might be interpreted as an improvement of properties of the theoretical curve with the improvement of the experimental data.

K. Desorption in Equilibrium

Since desorption is the process of reversing adsorption, the hypothetical desorption in equilibrium should just repeat the paths of adsorption isotherm curves without any changes (but in the inverse direction). Although, in real practice, as it was noted in Chapter 2, it is absolutely impossible to perform reversible adsorption–desorption on microporous adsorbents.

L. Thermoporometry

Thermoporometry is one of experimental methods for studies of microporosity. This method, the basis of which consists in the measurement of the vapor pressure and/or amounts of water vapor delivered from micropores under various temperatures, was analyzed in Chapter 2. Now, we can suggest a theoretical base for this method.

Since water evaporation from microporous adsorbents can be approximately considered as desoption close to equilibrium, Eqs. (4.34)–(4.36) are applicable. However, contrary to the adsorption isotherm case, thermoporometry uses the varied temperature.

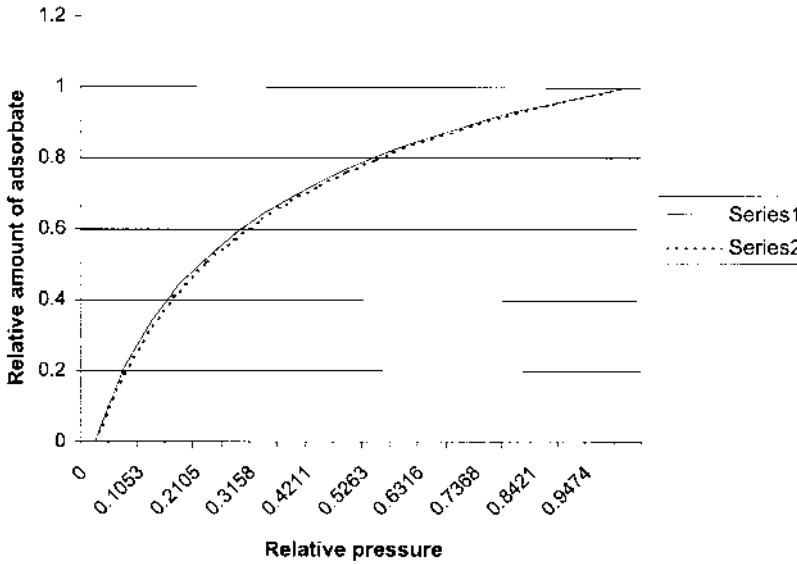

FIG. 4.10 Relative amount of adsorbate vs. relative pressure under varied temperatures. Series 1: Temperature 300 K; Series 2: Temperature 389 K.

Figure 4.10 presents thermoporometric curves for different temperatures: 300 K and 389 K. Since the total amount of adsorbate under the relative pressure = 1 depends much on the temperature, both curves were normalized (per the amount of adsorbate under $P/P_0 = 1$, that is, the relative amount of adsorbate) on purpose of detecting the sensitivity of the curve form to the temperature.

Table 4.2 illustrates the comparison between VFMT and Langmuir-like models.

M. Adsorption and Desorption in Nonequilibrium

All real processes of adsorption and desorption are irreversible and realized in nonequilibrium. The following factors cause nonequilibrium effects for adsorbent–fluid interactions [21]:

External diffusion: Limited velocity transfer of fluid molecules from the bulk fluid phase through a stagnant boundary layer surrounding each adsorbent particle to the external surface of the solid adsorbent – or back, in the case of desorption (limitation by fluid diffusion).

Internal diffusion: Limited velocity transfer of adsorbate molecules inside the adsorbent structure from fragments rich in the adsorbate

TABLE 4.2 Comparison Between VFMT and Langmuir-like Models

Criterion for comparison	VFMT	Langmuir-like
Suggested mechanism for pore–adsorbate interaction	Condensation approximation	Local Langmuir in volume
Suggested structure of micropores	Gauss distribution in size or energy	Determined by conditions of micropore formation
Accounting re-structuring (heterogeneity)	Gibbs distribution	Determined by conditions of microporous medium formation
Minimal number of fitted parameters (for homogeneity)	Two	Two
Number of fitted parameters for heterogeneity	Six	Two
Physical sense of fitted parameters	Empirical	Semiempirical
Principal accordance with experimental curves	Close	Identical

to fragments poor in the adsorbate, by the migration of the adsorbate molecules from the relatively small external surface of the adsorbent to the surfaces of the pores within each particle and/or by the diffusion of the adsorbate molecules through the pores of the particles—or back, for desorption (limitation by adsorbate diffusion).

Destruction and other irreversible changes of the adsorbent structure.

Eventual closing of narrow micropores with molecules of the adsorbate (or products of chemisorptive or catalytic reactions).

The problem of limitation by adsorbate diffusion will be considered below, in the part regarding phenomena of percolation and permeability in microporous materials. Phenomena concerning changes of the solid structure will be considered in Chapter 5.

Thus, the only thing we will touch here is the limitation by fluid diffusion, regarding the appearance of hysteresis loop.

The problem of mass transfer in fluids is widely studied in physical chemistry [2,21].

Let us consider the following scheme of fluid-diffusion-limited adsorption (see Fig. 4.11).

The adsorbed component G (its concentration C_G in the gas phase) comes slowly from bulk fluid to the solid–fluid interface and then penetrates (very fast) into micropores and becomes adsorbate. The concentration of G

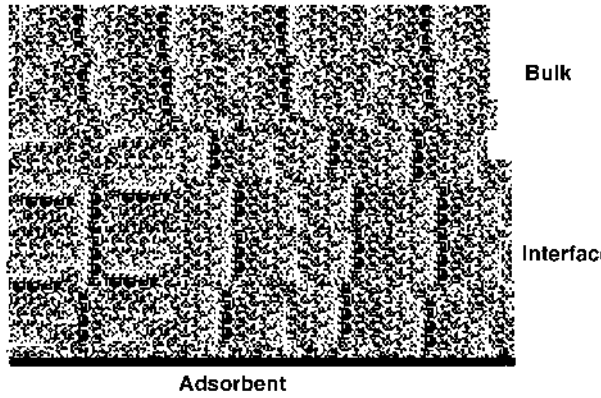

FIG. 4.11 Fluid-diffusion-limited adsorption–desorption.

at the interface is quasistationary ($C_{G,int}$) and in the bulk is constant ($C_{G,bulk}$). Of course, $C_{G,int} < C_{G,bulk}$. According to second Fick's law, such a quasi-steady-state situation is described by the following equation:

$$\Delta C_G = 0 \tag{4.37}$$

where ΔC_G means the sum of the second derivatives of C_G by the spatial coordinates. Assuming one-dimensional mass transfer, we simplify Eq. (4.37):

$$\frac{d^2 C_G}{dl^2} = 0 \tag{4.38}$$

where l is the distance from the adsorbent surface. The boundary conditions are $C_G(0) = C_{G,int}$, $C_G(L_b) = C_{G,bulk}$, L_b being the distance from the adsorbent surface to the zone of the fluid, where the local concentration is approximately equal $C_{G,bulk}$. The solution of Eq. (4.38) is linear:

$$C_G(l) = C_{G,int} + \frac{l(C_{G,bulk} - C_{G,int})}{L_b} \tag{4.39}$$

The entropy increase rate is proportional $(C_{G,bulk} - C_{G,int})^2$. The rate of the transfer is found from the following equation [2]:

$$J_G = \gamma_G A_{Ads} \omega_{Ads} \frac{C_{G,bulk} - C_{G,int}}{\rho_b} \tag{4.40}$$

where J_G is the flux of fluid particles toward the adsorbent surface, γ_G is the external film mass transfer coefficient, A_{Ads} is the external surface of particle of the fluid, ω_{Ads} is the voidage between adsorbent granules, and ρ_b is the bulk density of particle of the fluid [2]. The external mass transfer coefficient for the fixed-bed adsorber can be evaluated from empiric equations derived by Wakao and Funazkri, Petrovic, and Thodos [2].

Now, if the adsorption process is replaced by desorption in the same regime, the bulk concentration of G is $C^*_{G,bulk}$ (respectively, $C_{G,int} > C^*_{G,bulk}$), and the equation for $C_G(l)$ is

$$C_G(l) = C_{G,int} + \frac{l(C^*_{bulk} - C_{G,int})}{L_b} \tag{4.41}$$

The measured isotherm of desorption will exhibit hysteresis: the distance of the desorption isotherm from the adsorption isotherm will be $(C_{bulk} - C^*_{bulk})$. Hence, the surface area of the hysteresis loop in such situation brings us information about the kinetic characteristics of the process of adsorption–desorption limited by fluid diffusion.

As we noted above, the limitation by fluid diffusion is not alone but one of possible factors of hysteresis appearance. How can we distinguish it from other factors? If we intensify the motion of the bulk fluid (e.g., by a mixer) and then the hysteresis loop seems to become more narrow, it is the sure symptom that the process is limited by fluid diffusion.

II. PERCOLATION AND PERMEABILITY

A. Description of Percolation and Permeability

General and experimental aspects of percolation and permeability were considered in Chapter 2. Now, let us analyze theoretical aspects of these phenomena: first of all, existing theoretical models of percolation and permeability.

First of all, note that the physical nature of percolation and permeability in microporous materials is similar to adsorption–desorption. In both situation, some fluid interacts with pores located in a microporous medium, and the physics of related interactions can be given by Eqs. (4.8)–(4.11). On the contrary to adsorption, the fluid in a permeable medium may leave the solid structure, if that is not forbidden by structural factors. Hence, percolation can be considered as a simultaneous combination of adsorption and desorption: the fluid is adsorbed but immediately desorbed—and, due to the gravity factor, leaves the pores.

Of course, it is possible that some components of the fluid are not allowed to penetrate through the porous medium, and their behavior can be described as adsorption without further desorption.

B. Existing Models of Percolation and Permeability

All existing models of percolation–permeability are based on the idea of connectedness. That means that the empty (porous) substructure inside the solid is continuous from "entrance" to "exit," and its "thickness" from the entrance to the exit is always sufficient to allow the particles of the fluid to pass through the medium.

All existing models of percolation and permeability can be methodologically divided into three groups:

1. Models applicable to both percolation and permeability: theoretical tools allowing the solution of both problems—estimation of percolation threshold and quantitative evaluation of permeability over the percolation threshold
2. Models applicable only to percolation
3. Models applicable only to permeability

In principle, any restrictions in the applicability of a model are the symptom of its shortcomings. It is obvious that a well-built model of permeability allowing the evaluation of fluid fluxes through a porous sample should show also the conditions, under which these fluxes equal zero, which is the percolation threshold by definition. On the other hand, a model, describing a porous material below and exactly at the percolation threshold, should be able to do that over this one, bringing information about the permeability. Nevertheless, the above division of percolation–permeability models is the fact we need to take into account.

The following approaches and techniques are used in studies of percolation and permeability:

1. Darcy Equation

Darcy equation is a phenomenological approach in the description of permeability, based on Onsager equations (see Chapter 3). Darcy equation is usually written in the following form:

$$J_n = \frac{\sum_k^{N_f} g_{kn} X_k}{\eta_n} \tag{4.42}$$

where k and n label the phases and the fluid fluxes, I_n is linked to the pressure gradient (forces) X_k, g_{kn} are the permeability coefficients, and η_n is the ith fluid viscosity. As in Onsager equations, coefficients g_{kn} are characterized by reciprocity ($g_{nk} = g_{kn}$) investigated by Flekkoy and Pride [22].

The main shortcoming of the Darcy equation consists in the non-clear physical sense of the coefficients g_{kn}, which makes impossible evaluations of percolation threshold. If their relationship with microscopic properties of the porous material is studied, it is not problem to generalize this approach onto percolation (an example of such expansion is given below).

Another shortcoming of Darcy equation consists in its invalidity in situations when both the exterior pressure and the fluxes have short values. In such situation, the linear approximation is wrong, and the system is described by Chapman–Enskog equation considered below.

2. Chapman–Enskog Equation

In a specific case of a porous material interacting with little amounts of gas (so little that the interaction can be considered as physisorption), the rate of fluid current from the surface to the interior parts of the porous medium is generally controlled by transport within the pore network. Intraparticular transport is consider as a diffusive process, kinetic data of which correlate in terms of a diffusivity defined in accordance with Fick's first law of diffusion. Intraparticular diffusion may occur by several different mechanisms, comprising ordinary diffusion, molecular diffusion, Knudsen diffusion, or surface diffusion. The concrete mechanism depends on pore-size and pore-energy distribution, the fluid concentration inside the porous medium, etc. For a dense fluid inside macropores, the mechanism corresponds to the molecular diffusion. If the fluid is a gas phase with low density and/or the fluid is found in mesopores, the molecules collide with pore walls much more frequently than with each other, which is the mechanism of Knudsen diffusion. Molecules found of the surface may evidence a considerable mobility. The transport by the motion of molecules on a surface is known as *surface diffusion* [2]. The Chapman–Enskog equation for the effective molecular diffusivity in a gas–solid system is written in the following form:

$$D_m = \frac{[B_{ce} T^{3/2} (1/M_1 + 1/M_2)^{1/2}]}{(P a_{12}^2 \nu_{ce})} \tag{4.43a}$$

$$B_{ce} = 10^{-4} \left[10.85 - \frac{2.5}{(1/M_1 + 1/M_2)^{1/2}} \right] \tag{4.43b}$$

where D_m is the molecular diffusivity, M_1 and M_2 are the molecular masses, P is the total pressure, $a_{12} = (a_1 + a_2)/2$ is the collision diameter from the Lennard-Jones potential (A), ν_{ce} is a function of $[\varepsilon_{ce}/(k_b T)]$, and $\varepsilon_{ce} = (\varepsilon_1 \varepsilon_2)$ is a Lennard–Jones force constant.

As Darcy equation, Chapman–Enskog equation does not allow the estimation of percolation threshold. Methodologically, these equations complete one other: for short pressures Chapman–Enskog equation works, for moderate and high pressure Darcy equation is valid.

3. Monte Carlo Simulations

This approach is based on the assumption that the motion of particles in the system is random, and there is no relationship between the current state of the system and its prehistory [23]. Monte Carlo modeling of fluid motion means that each element of the fluid flow can eventually penetrate into each of available fragments of the solid medium with the probability determined by some assumptions taken by the researcher, and then the appearance of percolation path(s) is confirmed or denied. Monte Carlo can be employed also for modeling of microporous structure formation by a casual mechanism, this aspect is considered in Chapter 5. In many cases, Monte Carlo simulations are performed on computer and do not provide analytical solutions. In principle, Monte Carlo approach is applicable to both percolations and permeability problems, but the absence of analytical solution reduces its usefulness.

4. Infinite Cluster (Fractal) Approach

This approach is based on the fractal concept, some aspects of which were already considered in Chapters 1 and 3. A percolation cluster is assumed to consist of porous clusters described as fractals of finite size or infinite. The main idea of the infinite cluster approach is that percolation is due to the formation of an infinite connected porous structure. This model was found useful in characterizing many types of disordered systems (not only solids), e.g., gels, fractures, dispersed ionic conductors and mixed alkali conductors, forest fires, and epidemics [24]. The site percolation in the infinite percolation cluster model is defined by choosing each site of the lattice to be occupied with a probability Pr (or, respectively, to be found empty with probability $(1 - \mathrm{Pr})$). A similar definition exists for bond percolation. There exists a critical value of Pr, $\mathrm{Pr_c}$, below which only finite-size clusters exist and above which an infinite cluster is generated. For a triangular lattice, $\mathrm{Pr_c} = 1/2$. For a square lattice, it was found numerically that $\mathrm{Pr_c} = 0.592745$ [24]. The percolation transition at $\mathrm{Pr_c}$ is described by the probability $\mathrm{Pr_{inf}}$

that a site in the lattice belongs to the cluster. Below Pr_c, $Pr_{inf} = 0$, whereas above Pr_c, Pr_{inf} increases with Pr [24]:

$$Pr_{inf} \sim (Pr - Pr_c)^{b_c} \tag{4.44}$$

where b_c is a parameter.

The diameter of the clusters below Pr_c is characterized by the correlation length λ, which can be understood as the mean distance between two sites belonging to the same cluster. When $Pr \to Pr_c$, $\lambda \to (Pr_c - Pr)^{-\nu_c}$. The parameters b_c and ν_c are universal and depend only on the fractal dimensionality d_f (this is a main characteristic of the dimensionality of fractals; this question will be considered in Chapter 5 in more details). The infinite cluster for $Pr > Pr_c$ can be modeled as a regular lattice of fractal unit cells. Each fractal unit cell is of linear size $\lambda(Pr)$ and is similar to the fractal lattices modeling percolation at $Pr < Pr_c$ [24]. Diffusion in a percolation structure can be generated, in the infinite cluster model, by performing a random walk which can step only on the occupied sites belonging to the clusters (note that this detail attributes to infinite cluster models some features of Monte Carlo). The boundary unoccupied sites serve as reflecting sites. For $Pr < Pr_c$, the random walk is constrained to stay on the finite clusters and therefore its mean square displacement will increase with time until it reaches a plateau value characteristic of the linear size of the cluster, on which the random walk started. For $Pr > Pr_c$, for a random walk that started on the infinite cluster, its mean square displacement will increase with time [24].

The infinite cluster approach is applicable to both percolation and permeability problems: the percolation threshold is found from the value of Pr_c, and fluid current passing through the porous structure is related to Pr_{inf} in Eq. (4.44).

Let us observe some shortcomings of the infinite-size cluster approach:

As all fractal models, the infinite-size cluster approach does not take into account the specificity of pores. Are they ultramicropores, supermicropores, mesopores—the result will be the same. Even the difference between open, semiopen, and closed pores is not taken into account anyway, though the predomination of semiopen or closed pores will obviously restrict any percolation.

Since this model requires the infinite size for the percolation cluster, the resulting value of parameters of percolation threshold will be overestimated. For big samples this overestimation can be negligible, but for thin films Eq. (4.44) will provide absurd overestimation.

In the estimation of permeability, Eq. (4.44) provides the problem of taking into account the specificity of different fluids.

5. Pore-Size Distribution Approach

This approach is based on the obvious assumption that pore size determines the permeability of porous structure, hence, pore-size distribution (PSD) determines the total percolation–permeability properties of the system [25–30].

We can notify two principal shortcomings in PSD method:

As we wrote in Chapter 1, the sense of pore size is extremely unclear in the case of micropores; in any case, micropore size cannot be directly measured or calculated from experimental data.

Fluid–solid interactions in porous fractals are determined not only by the geometrical factor (pore size) but also the compatibility between the fluid and pore wall material.

6. "Pore-Core" Model

This approach is empirical. The main idea consists in the estimation of the relationship between different measurable parameters, e.g., percolation and permeability characteristics and Hg-intrusion results [31,32].

In principle, the relationship between all measurable parameters of porous structures is doubtless (see more details on this subject in Chapter 1), but the empirical representation of this relationship has all shortcomings of empirical methods. In principle, the researcher using empirical approach can never be sure what happens in the zone of properties not yet measured, cannot evaluate the errors of the approximation, etc.

7. Finite-Size Cluster Approach

The finite-cluster approach in modeling percolation and permeability is based on the assumption that experimental research deals not with infinite porous samples but some pieces having limited size (in the case of films this size can be very short) and corresponds to the situation given on Fig. 1.1 (see Chapter 1).

The finite-size cluster approach is based on the following assumptions [33]:

The primary sample of microporous material (not for tests!) is prepared in the form of a very big cube—so big that border effects are negligible. In such case, the sample may be considered as homogeneous system, and the Law of Large Numbers is applicable;

The sample for percolation–tortuosity tests (secondary, or tested sample) is a small cube (size L) eventually taken from the primary sample.

As follows from results presented in Chapter 3, micropore formation in the primary sample leads to the appearance of porous clusters of varied volume and surface, but all they have the same geometrical form as the primary sample. Hence, they are cubes, though their fractal dimensionalities differ. Each cluster is characterized by volume V and one of the following parameters: fractal dimensionality d_f, surface area A, or size D. Clusters are distributed in V and $d_f/A/D$, the distribution function being $\psi(\mathrm{V},d_f) = \psi(\mathrm{V},A) = \psi(\mathrm{V},D)$. The correlation between these parameters is given by [33]

$$V = D^{d_f}, \qquad A = 2d_f D^{(d_f - 1)} \tag{4.45}$$

Percolation effect is observed for the tested sample if two following conditions are completed:

The tested sample having size L is totally or partly taken from a microporous structure containing cluster with the size $D > L$.

The distance from the geometrical center of the tested sample to each point belonging to the border of the mentioned cluster is at least $L/2$.

According to the criteria proposed above, certain (nonzero) percolation in the tested sample is always possible, because all methods of microporous material preparation may eventually cause formation of big clusters that may eventually become zones from which the tested sample are taken. Moreover, percolation cluster does not need large volume; it is enough if its dimensionality is short (close 1 as possible). The probability of eventually taking the tested sample from a cluster with characteristics (V, D) is

$$P(V, D) = \left(1 - \frac{L}{D}\right)\psi(V, D) \tag{4.46}$$

For a heterogeneous structure, the total probability of appearance of percolation for the tested sample is given by [33]

$$P_\Sigma = \int_{d_{f,\,\min}}^{d_{f,\,\max}} \int_{V_{\min}}^{V_{\max}} Q_0 \left[1 - \frac{L}{D(V, d_f)}\right] \psi(V, d_f)\, dV\, d(d_f) \tag{4.47a}$$

where Q_0 is the normalizing coefficient, $d_{f\min}$ and $d_{f\max}$, $V_{\min}$ and $V_{\max}$ are minimum and maximum values of fractal dimensionality and cluster volume, respectively. For a homogeneous structure, $d_{f,\min} = d_{f,\max}$. One may also assume $V_{\min} = L^{d_{f,\min}}$, $V_{\max} = \infty$ [33].

Let us note that, as follows from Eqs. (4.46) and (4.47a), depending on the conditions of preparation of microporous material determining the value of ψ, percolation can be sometimes gained in samples having low porosity.

The value of the normalizing coefficient Q_0 is found from the following condition:

$$\int_{d_{f,\min}}^{d_{f,\max}} \int_{V_{\min}}^{V_{\max}} Q_0 \psi(V, d_f)\, dV\, d(d_f) = 1 \tag{4.47b}$$

The value ψ is found from energy distribution of pores, as it is done in Chapter 3.

Let us consider clusters enclosed in several fragments of structure of the primary sample. These fragments contain particles of the continuous solid phase, which may be very near the enclosed clusters. In principle, inside such a fragment containing "exterior" cluster one may find some other fragments containing "interior" clusters of shorter size. We note that in such situations external clusters may eventually have less volume (because of shorter dimensionality) than internal ones.

The total values of the volume and the surface area of the porous phase are found from [33]

$$V_\Sigma = \int_{d_{f,\min}}^{d_{f,\max}} \int_{V_{\min}}^{V_{\max}} Q_0 V \psi(V, d_f)\, dV\, d(d_f) \tag{4.48a}$$

$$A_\Sigma = \int_{d_{f,\min}}^{d_{f,\max}} \int_{V_{\min}}^{V_{\max}} Q_0 A \psi(V, d_f)\, dV\, d(d_f) \tag{4.48b}$$

In the light of the considered approach, the sense of such notions as percolation threshold and permeability also changes. Percolation threshold should be considered as such minimum of probability of percolation [that is found from Eq. (4.47)] that below this threshold percolation is neglected, according to the practical interests of the researcher. Permeability is estimated from Eq. (4.47), while tortuosity is found from the equation [33]

$$\tau = \frac{D^3}{(VLP_\Sigma)} \tag{4.49}$$

Now, let us analyze shortcomings of the finite-size cluster model. In comparison with the infinite-size cluster model, the finite-size cluster model solves the problem of short size and can be, in principle, applied to films. Although, the problem of taking into account the specificity of micropores remains. Also the problem of different fluids (that should influence the value of P_Σ when this is interpreted as permeability) stays without solution.

8. Random Trajectory Model for Percolation (Slab Symmetry)

As the finite-size cluster method can be methodologically considered as a development of the infinite-size cluster approach, the random trajectory approach can be considered as a development of the finite-size cluster method. As in this one, the random trajectory method is based on the idea of the finite path needed for the percolation effect. However, the random trajectory method considers not fractals but pores themselves—moreover, the solid particles belonging to the continuous phase. In this sense, the random trajectory method should be considered as a discrete model of porous solid structure.

The random trajectory method considers the solid structure, in the simplest situation, as a slab having thickness L, with the microporous structure having porosity ξ and divided into cells: filled cells belonging to the continuous phase or empty cells (voids) belonging to the porous medium (that can be compared to Pore-Core). As it was shown in Chapter 3, filled cells are distributed in the number of empty neighbors, and this distribution can be found from differential equations containing the formation-related parameters like surface tension σ and temperature T.

Similar equations can be written for the analogous distribution of empty cells. Since interface and entropy effects have a symmetric form against both filled and empty cells, the number of voids having $(n_n - m)$ empty neighbors at porosity ξ_1 ($\xi_1 = V_2/V_\Sigma$, where V_Σ is the total volume of the system) is equal to the number of filled cells having m empty neighbors at porosity $\xi_2 = \xi = (1 - \xi_1)$. Hence, we obtain the corresponding distribution of voids $\theta_m(\xi)$, m being the number of empty neighbors; θ_m is equal to the fraction of voids having (each) m empty neighbors: $\theta_m(\xi) = \nu_{(n-m)}(1 - \xi)$. The change of the distribution of voids in the number of empty neighbors is given by the following equations:

$$W_r(m) = Q_0 m \exp\left[\frac{-\sigma(n_n - m)}{R_g T}\right] \tag{4.50}$$

$$d\theta_m(V_{\text{pore}}) = W_r(m)\, dV_{\text{pore}} + \frac{\psi\, dV_{\text{pore}}[\theta_{m-1}(n_n - m + 1) - \theta_m(n_n - m)]}{Z_\Sigma} \tag{4.51}$$

$$Z_\Sigma = \sum_{k=0}^{n_n-1} (n_n - k)\theta_k$$

$$\psi = \sum_{k=0}^{n_n-1} (n_n - k)\theta_k \frac{\exp[-\sigma(n_n - k)/(R_g T)]}{Y_\Sigma}$$

$$Y_\Sigma = \sum_{k=0}^{n_n-1} \theta_k \exp\left[\frac{-\sigma(n_n - k)}{(R_g T)}\right]$$

$$d\theta_0(V_{\text{pore}}) = \frac{dV_{\text{pore}}\psi\theta_0 n_n}{\sum_{k=0}^{n_n-1} (n_n - k)\theta_k} \tag{4.52}$$

$$d\theta_{nn}(V_{\text{pore}}) = -W_r\, dV_{\text{pore}} + \frac{dV_{\text{pore}}}{\sum_{k=0}^{n_n-1} (n_n - k)\theta_k} \tag{4.53}$$

We assume that the orientation of empty neighbors for voids is eventual, meaning all orientations being possible with the same probability, while the percolating flow prefers the orientation "down." If this one is impossible, the flow prefers a horizontal orientation, and only in the case where the only open orientation is "up," the flow gets up. If the flow has "choice" between different trajectories, it "prefers" the shorter way (shorter in comparison with alternative trajectories).

The motion of the percolating flow is only through the voids having at least two empty neighbors. Let us characterize each void by its level h, the distance from the upper size of the considered cube; for the upper size, $h = 0$, and for the bottom, $h = L$. For neighbor cells on the same vertical, h differs by 1.

There are three principal options for the motion of the flow from a void located on level h into a void on a close level h' [34]:

1. $h' = h + 1$, the flow gets down, and its further motion has two options only: down or horizontally (obviously, because the upper orientation is already closed by the incoming flow). The option down is obtained if the considered void on level h' has an empty neighbor on level $h'' = h' + 1$, this probability is equal to $(m-1)/(n_n - 1)$, where n_n is the coordination number (for a three-dimensional cube, $n_n = 6$, for a two-dimensional cube, $n_n = 4$).

Respectively, the probability of the horizontal motion is $(n_n - m)/(n_n - 1)$.

2. $h' = h$, the flow gets horizontal trajectory, and its further motion has three options:
   a. Down, with the probability $(m-1)/(n_n - 1)$.
   b. Horizontally, with the probability $(n_n - m)/(n_n - 1)$ in condition that $m > 2$.
   c. Up, only if $m = 2$ and the orientation down is closed.
3. $h' = h - 1$, the flow gets up, and its further motion has two options only: up or horizontally. The option up is obtained only if $m = 2$ and the only open orientation is up; otherwise, that is a horizontal motion.

Now, let us consider a percolation way comprising l_+ acts of motion down, l acts of motion up (certainly, $l_+ - l_- = \mathrm{L}$), and l_0 acts of horizontal motion. Some examples of percolation paths are given on Fig. 4.12.

Let us note that the sequence of the acts of motion up, down, and horizontally has no importance. The total length of such percolation way is $l^* = l_+ + l_- + l_0$, and the percolation system gets two factors of freedom: l_0 and l^*.

The probability of an act of motion down is [34]

$$p_+ = \varsigma \sum_{m=2}^{n_n} \theta_m \frac{m-1}{n_n - 1} \tag{4.54}$$

The total probability of the walk l_+ down is $(p_+)^{l+}$.

The probability of each act of motion up is

$$p = \frac{\xi \theta_2}{n_n - 1} \tag{4.55}$$

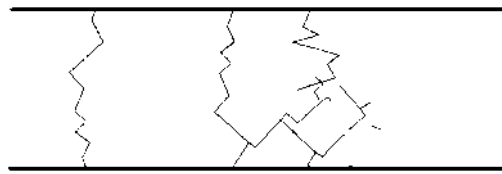

FIG. 4.12 Variants of percolation paths.

The coefficient $1/(n_n-1)$ is written in Eq. (4.55), because only the $1/(n_n-1)$-th part of the situation $m=2$ allows the orientation up. The total probability of the walk l_- down is (p_-).

The geometrically averaged probability of each act of horizontal motion is [34]

$$p_0 = \frac{\xi(l_+ - l)\,S_1 + (l_0 - l)(S_2 + S_3) + (l - S_4)}{(l^* - 2)} \tag{4.56}$$

$$S_1 = \sum_{m=2}^{n_n} \theta_m \frac{(n_n - m)}{(n_n - 1)}$$

$$S_2 = \sum_{m=3}^{n_n} \theta_m \frac{(n_n - m)}{(n_n - 1)}$$

$$S_3 = \frac{\theta_2}{n_n - 1}$$

$$S_4 = \frac{\theta_2/(n_n - 2)}{n_n - 1}$$

We note that p_0 depends on l^* and l_0, because horizontal orientation has much more options for realization than vertical. The total probability of horizontal walk l_0 is $p_0^{l_0}$.

The probability of a percolation trajectory having parameters (l^*, l_0) is found from the following equation [34]:

$$P(l^*, l_0) = p_+^{l_+} p_0^{l_0} p_-^{l_-} \tag{4.57}$$

The total probability of percolation is found as the sum over all possible percolation trajectories [34]:

$$P_\Sigma = \sum_{l_1=L}^{l_{\max}} \sum_{l_2=0}^{l_1-L} P(l_1, l_2) \tag{4.58}$$

where l_1 and l_2 have the sense of l^* and l^0, respectively, and $l_{\max}$ is the maximal possible walk corresponding to all voids forming the same percolation way, found as follows:

$$l_{\max} = \xi \frac{V_0}{(w_0)^{2/3}} \tag{4.59}$$

where $\omega_0 = 1$ is the volume of a cell.

Comparing the obtained solution to the finite-size cluster model, we note that different percolation trajectories may belong to different clusters. The condition of the conjugation of the obtained solution with the cluster model is given as follows:

$$P_{\Sigma 1} = P_{\Sigma 2} \tag{4.60}$$

$$P_{\Sigma 1} = \sum_{l_1=L}^{l_{\max}} \sum_{l_2=0}^{l_1-L} P(l_1, l_2) \tag{4.61}$$

$$P_{\Sigma 2} = \int_{f_{\min}}^{f_{\max}} \int_{V_{\min}}^{V_{\max}} Q_0\left(1 - \frac{L}{D(V,f)}\right) \Psi(V,f)\, dV\, df \tag{4.62}$$

where all values regarding the finite-size clusters have the same sense as in the previously considered model.

Thus, the random trajectory model allows the prediction of percolation threshold from the distribution of empty cells in the number of empty neighbors. This model takes into account the finite size of the real porous structure and closing or semiopening of pores. However, the above model is not still appropriate for estimations of permeability.

9. Random Trajectory Model for Permeability (Slab Symmetry)

This version of the random trajectory model assumes that all percolation trajectories (for which $l_+ = l_- + L$) contribute passing through of the fluid flow. The total capability of random trajectories to allow the penetration of the fluid from the head to the bottom of the sample determines the permeability properties of the solid structure. For hydraulic reasons, the shapes of the paths are not important for the fluid penetration rate.

Thus, in the random trajectory model for permeability, this is considered as the result of the motion of a fluid along percolation paths. The principal difference between both versions of the random trajectory model (percolation and permeability versions) consists in the absence of preferable orientations: for hydraulic reasons, all available orientations have the same probability to get the fluid flow. Each percolation path begins at the head of the considered sample and finishes at its bottom. Each percolation path is characterized by the values of l_Σ and l_0 and the sequence of steps down, horizontally, and up. At the same pair (l_Σ, l_0), the variety of

percolation paths is numerically characterized by the number of possible combinations. This is found as

$$g(l_\Sigma, l_0) = C_{l_\Sigma}^{l_+} C_{l_\Sigma - l_+}^{l_-} \tag{4.63}$$

where $C_{l_\Sigma}^{l_+}$ is the number of possible placements of l_+ steps down among l_Σ steps totally and $C_{l_\Sigma - l_+}^{l_-}$ is the number of possible placements of l_- steps up among $l_\Sigma - l_+$ steps remaining after steps down.

For a chosen trajectory characterized by the pair (l_Σ, l_0), the probability of its availability for percolation is determined by the following factors [35]:

All cells belonging to the same percolation path must be empty (probability of such event is ς^{l_Σ}).

Each of these cells needs at least two empty neighbors (probability of such event is $[(1-\theta_0)\ (1-\theta_1)]$, where θ_μ is the number of voids having (each) μ empty neighbors.

The values of θ_0 and θ_1 are found from the same equations as written for the random trajectory model for percolation.

The total intensity of the flow penetrating through the sample per unit of surface area is [35]

$$\Pi_f = \sum_{l_\Sigma = L}^{l_{\max}} \sum_{l_0 = l_{\min}}^{l_\Sigma - L} g(l_\Sigma, l_0)\pi(l_\Sigma, l_0) \tag{4.64}$$

$$\pi(l_\Sigma, l_0) = \varsigma^{l_\Sigma}(1-\theta_0)^{l_\Sigma}(1-\theta_1)^{l_\Sigma} A_{\theta_1} A_{\theta_2} \tag{4.65}$$

$$A_{\theta_1} = \left[\sum_{m=2}^{n_n} \frac{\theta_m m(m-1)}{n_n} \right]^{l_+ + l_-} \tag{4.66}$$

$$A_{\theta_2} = \left[\sum_{m=2}^{n_n} \frac{\theta_m m(n_n - 2)}{n_n} \right]^{l_0} \tag{4.67}$$

The resistance of $(l_\Sigma,\ l_0)$-th trajectory to the flow is determined not by its shape, not by the sequence of steps, but only by the length of the trajectory. The pressure needed for the flow passing through is

$$\delta P = \eta l_\Sigma \omega(l_\Sigma) \tag{4.68}$$

where $\omega(l_\Sigma)$ is the linear velocity of the flow inside a path having the total length l_Σ, and η is the friction coefficient. The amount of the fluid penetrating through the sample is [35]

$$\Theta_f = \sum_{l_\Sigma=L}^{l_{\max}} \sum_{l_0=l_{\min}}^{l_\Sigma-L} \omega(l_\Sigma) g(l_\Sigma, l_0) \pi(l_\Sigma, l_0) \tag{4.69}$$

From Eqs. (4.68) and (4.69) we obtain

$$\Theta_f = \sum_{l_\Sigma=L}^{l_{\max}} \sum_{l_0=l_{\min}}^{l_\Sigma-L} \frac{\delta P g(l_\Sigma, l_0) \pi(l_\Sigma, l_0)}{(\eta l_\Sigma)} \tag{4.70}$$

Equation (4.70) can be considered as Darcy equation for microporous medium [compare to Eq. (4.42)].

An analysis performed in Ref. 35 on the base of Eq. (4.70) showed that nonzero permeability is found even for very low porosity, but there is a very narrow interval of values of the porosity, in which the value of Π_f gets a very sharp rising. This regime corresponds to Π_f getting value up to 1 and can be called *visible percolation threshold* (VPT), because it is the parameter really available for experimental measurements. The notion of VPT is commendable for the characterization of permeability properties.

It was shown in Ref. 35 that VPT decreases with rising of the coordination number n_n, because of the increase of the number of parameters of freedom in the system, and Π_f increases.

Also, the influence of connectedness [numerical definition of which is given in Chapter 2] was studied in Ref. 35. It was shown that the increase of connectedness first reduces much VPT, but then has almost no influence.

The influence of thickness also was analyzed in Ref. 35. It was shown that, though VPT always increases with thickness (that is normal), the derivative of this increase is negative.

Thus, the random trajectory approach allows the solution of all problems related to percolation and permeability. The principal comparison of various methods of characterizing percolation and permeability is illustrated by Table 4.3.

Thus, the random trajectory method is definitely commendable for the solution of traditional problems related to percolation and permeability.

TABLE 4.3 Applicability of Existing Methods of Modeling Percolation and Permeability

Method or model	Sphere of applicability	Physical sense of the method	Limitations or shortcomings of the method
Darcy equation	Permeability only	Linear thermodynamics, Onsager equations	Applicable only over percolation threshold; applied pressure needs to be high enough
Chapman–Enskog equation	Permeability only	Linear thermodynamics of diffusion in multi-particle system	Applicable only over percolation threshold; applied pressure needs to be short enough
Monte-Carlo simulations	Both percolation and permeability	Chaos in particle motion	Pre-history of the system not taken into account
Infinite cluster approach	Both percolation and permeability	Infiniteness of the co-existing fractals	Not applicable to films
Finite-size cluster approach	Both percolation and permeability	Finite size of co-existing fractals	Specificity of micropores not taken into account
PSD	Both percolation and permeability	Pore-size distribution assumed	Difficulties in estimation of pore-size distribution for micropores
Pore-Core	Both percolation and permeability	Semiempirical correlations between measurable properties	Absence of fundamental solution
Random trajectory approach	Both percolation and permeability	Finiteness of percolation paths	Difficulties in studies of big solid samples

10. Random Trajectory Method for Modeling Permeability of System Having Sphere Symmetry (Heterogeneous Catalysis)

Now, let us use the random trajectory method for the solution of such practically important problem as the estimation of permeability of sphere. Such problem appears, particularly, in heterogeneous catalysis. The principal scheme of a catalytic particle is presented on Fig. 4.13.

The catalytic particle consists of two parts: the exterior sphere (porous carrier of the catalyst) and the interior sphere (porous catalytic nucleus). The exterior sphere (usually prepared of aluminium oxide or silica dioxide) aims to protect the catalytic nucleus (this can be prepared of precious materials, e.g., platinum, palladium) from eventual mechanical damage and chemical pollution. Catalytic particles are usually treated in the regime of fluidized bed (turbulent fluid flow coming from the bottom makes solid particles fly), they collide and make contact with walls, products of reaction, etc. If catalytic nucleus was unprotected, it would be destroyed and/or contaminated very fast.

The reagents from the exterior fluid flow penetrate into the carrier (exterior sphere having radius R) and pass through the pores of the exterior sphere into the catalytic nucleus (interior sphere with radius r), where the main reaction is performed. The products of the reaction are removed through the same pores of the carrier. Thus, the effectiveness of the catalytic process depends much on the permeability of the carrier.

As in the case of slab sample, the permeability is determined by percolation trajectories. However, in the considered situation, percolation

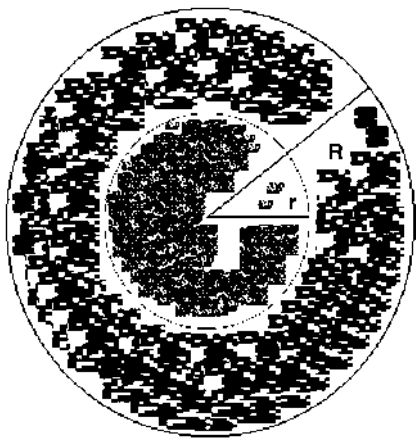

FIG. 4.13 Principal scheme of catalytic particle.

trajectories begin at the surface of the exterior sphere and finish at the surface of the interior sphere. Percolation path comprises l_+ steps toward the sphere center, l_- steps back (toward the exterior sphere surface), and l_0 steps in the plate perpendicular the radius vector, on which steps toward the center and back are measured. The motion perpendicular to the radius vector is characterized by two coordinates (see Fig. 4.14), as in the traditional consideration of three-dimensional space: steps parallel to the radius vector correspond to the direction Z, and perpendicular to the radius vector correspond to directions X, Y, and their combinations.

The percolation takes place, if

The balance of steps along the Z axis toward the center and back satisfies the condition

$$l_+ - l_- = R - r; \tag{4.71}$$

The balances of steps along X and Y axes in directions "plus" and "minus" allow getting the target (the catalytic nucleus) hence, their absolute values remain in the limit given by the interior radius r;

$$|l_{1+} - l_{1-}| \le r, \qquad |l_{2+} - l_{2-}| \le r \tag{4.72}$$

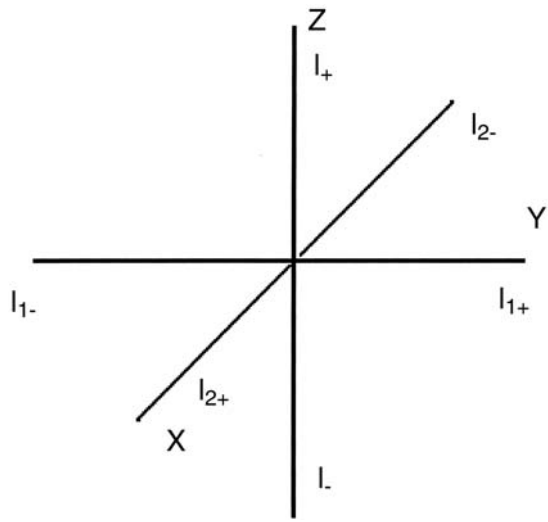

FIG. 4.14 Scheme of the choice of coordinates for the motion of flow through porous catalytic sphere.

Each percolation path is characterized by the group of five independent parameters: the total length (l_Σ), l_+, l_{1+}, l_{1-}, and l_{2+}. Their relationship is, obviously,

$$l_\Sigma = l_+ + l_- + l_{1+} + l_{1-} + l_{2+} + l_{2-} \tag{4.73}$$

As in the case of slab, the sequence of steps is not important (while, in principle, steps perpendicular the radius vector are constrained by the border of the exterior sphere). At the same values of these parameters, the number of possible combinations of percolation paths is found from the following equation:

$$g(l_\Sigma, l_+, l_{1+}, l_{1-}, l_{2+}) = C_{l_\Sigma}^{l_+} C_{(l_\Sigma - l_+)}^{l_{1+}} C_{(l_\Sigma - l_+ - l_{1+})}^{l_{1-}} C_{(l_\Sigma - l_+ - l_{1+} - l_{1-})}^{l_{2+}} \tag{4.74}$$

where the value C_n^m has the sense (as for the slab symmetry) of the number of possible placements of m steps among n available cells. The maximal length available for percolation path is equal numerically to $l_{\max +} = 4\pi(R^3 - r^3)/3$. The total intensity of the flow penetrating from the surface of the exterior sphere to the surface of the interior sphere is given by Eq. (4.64), and the total current getting to the catalytic nucleus is

$$J_\Pi = 4\pi R^2 \sum_{l_\Sigma = R-r}^{l_{\max}} \sum_{l_0 = 0}^{l_\Sigma - (R-r)} g(l_\Sigma, l_+, l_{1+}, l_{1-}, l_{2+}) \pi(l_\Sigma, l_0) \tag{4.75}$$

where $l_0 = l_\Sigma - l_+ - l_-$, as in the case of slab symmetry.

The results of calculations of various parameters related to the permeability of particle having a sphere symmetry are presented below on Figs. 4.15–4.16.

Figure 4.15 presents the appearance of VPT for a structure having sphere symmetry (like a catalytic particle).

As follows from Fig. 4.15, as in the case of slab symmetry, the permeability is very sensitive to the value of porosity, and a very sharp rising of the flow through the exterior sphere is found in a very narrow interval of values of porosity. As in the case of slab symmetry, this allows us to talk about visible percolation threshold (VPT) corresponding to the really measurable percolation. An experiment performed in conditions corresponding to these for Fig. 4.15 would bring us the result: percolation threshold corresponds to porosity about 0.617.

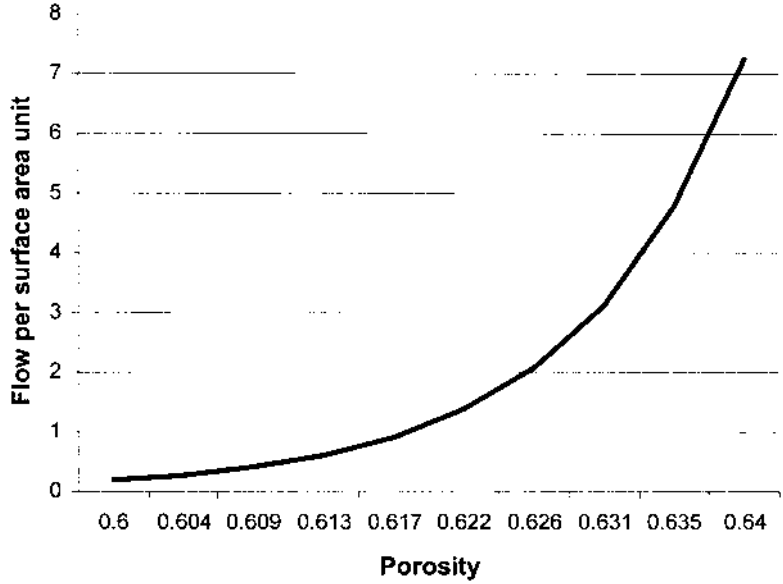

FIG. 4.15 Appearance of visible percolation threshold (VPT) for sphere symmetry, coordination number 6, $\varphi = 1$, $R = 15$, $r = 5$.

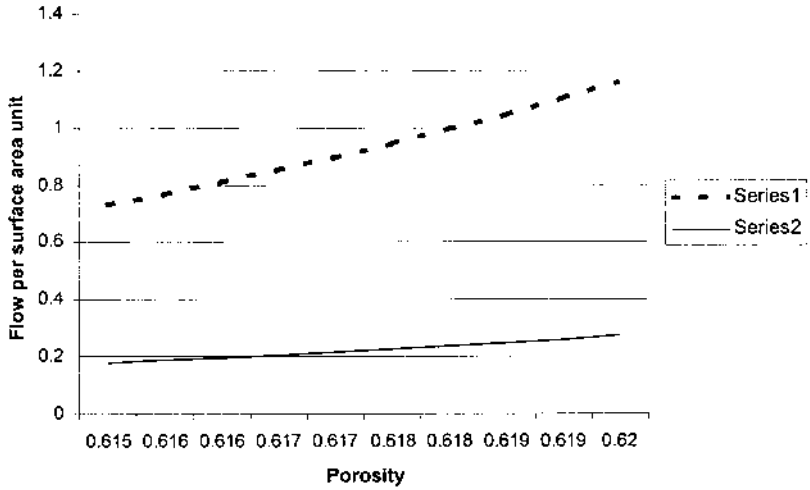

FIG. 4.16 Mass-transfer for heterogeneous catalysis: appearance of VPT for varied coordination number: Series 1: $n_n = 6$, Series 2: $n_n = 4$.

In the further analysis, we will characterize all parameters related to percolation threshold by their relationship with VPT, meaning the corresponding porosity, for which the flow per *exterior* surface unit is equal 1 (on all graphs, the text *flow per surface area unit* means the exterior surface).

Figure 4.16 presents the relationship between the permeability of sphere and the coordination number of particles (n_n); $n_n = 4$ corresponds to the plate situation (two-dimensional case) and $n_n = 6$, to the space (three-dimensional situation).

Figure 4.16 brings us a trivial result: the permeability depends much on the coordination number. This fact is doubtless, because the coordination number influences the degrees of freedom of the system: larger is the coordination number, more the flow has options for its motion, larger is the resulting flow through the medium. A similar result was obtained also for the slab symmetry.

Figure 4.17 presents the relationship between the permeability and the connectedness parameter φ.

As follows from Fig. 4.17, the connectedness parameter φ influences the value of VPT. Increase of the connectedness parameter reduces VPT

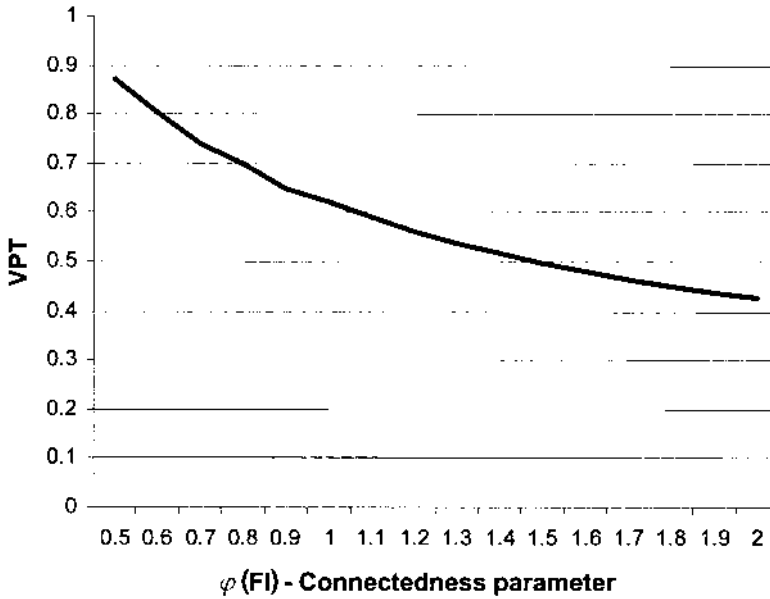

FIG. 4.17 Permeability as function of connectedness for sphere.

and, respectively, increases the permeability. In the physical point of view, this is because more regular structure (caused by high surface tension and corresponding to high values of the connectedness parameter) allows the easier penetration of the flow through the porous medium.

Very important, in the aspect of computing, is the question about the real value of l_{max} needed to be accounted in Eqs. (4.71)–(4.75). If the value is assumed very large, the calculation is very precious but takes extremely long time. If it is very short, the calculation is very fast, but the error of such calculation is too large. Figure 4.18 presents the calculated VPT vs. various values of (l_{max}/R).

As follows from Fig. 4.18, for $l_{max}/R \geq 2$, the error in the estimation of VPT becomes negligible. Therefore, all calculations of VPT presented above and below are made with the assumption that $l_{max}/R = 2$.

Now, let us analyze the influence of specific parameters of sphere onto the permeability. The sizes of the considered system can be characterized by a pair of parameters taken from the following list: r, R, (r/R). Let us choose the pair (r, R).

Figure 4.19 presents the relationship between the exterior radius (R) and VPT.

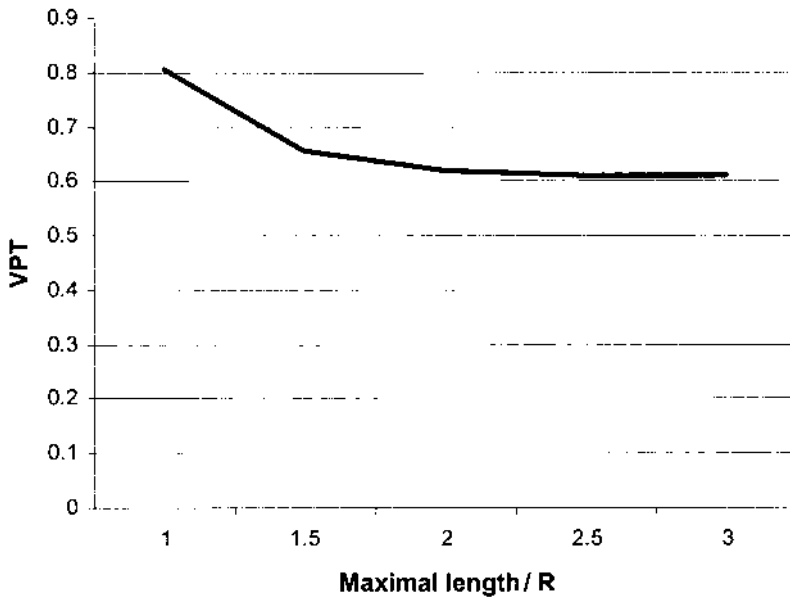

FIG. 4.18 Influence of the accounted length onto VPT calculated.

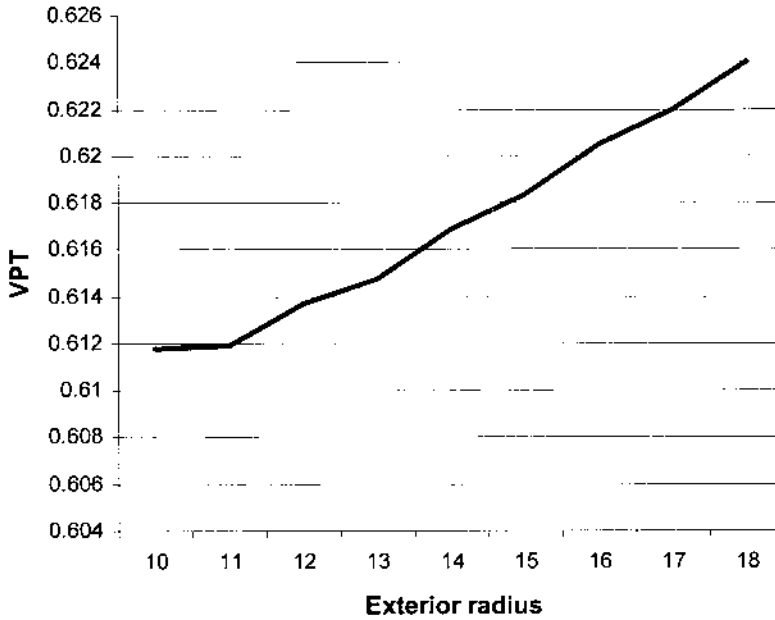

FIG. 4.19 Influence of the exterior radius on VPT.

As follows from Fig. 4.19, VPT increases with R. This result seems obvious, because the increase of R reduces the chance for a path beginning on the exterior surface to finish on the interior surface.

The influence of the interior radius r (radius of the catalytic nucleus) on VPT is given on Fig. 4.20.

As follows from Fig. 4.20, VPT decreases with r—for the same reason that VPT increases with R.

A parameter very important for practical needs is the total flow through the exterior surface found from Eq. (4.75), that is, the parameter presenting the technical merit of the catalytic system. As follows from Eq. (4.75), two factors compete: rising of R increases VPT, but also the total surface area increases!

Figure 4.21 presents the relationship between the total flow and the exterior radius. As follows from Fig. 4.21, the total flow passes through maximum with rising R. Why ? the total decrease of the flow when R is very large is obvious: because of the increase of VPT. Why the total flow increases to maximum for moderate values of R, that is, due to the increase of the exterior surface area: the large number of flows compensates the loss in the intensity of each of them.

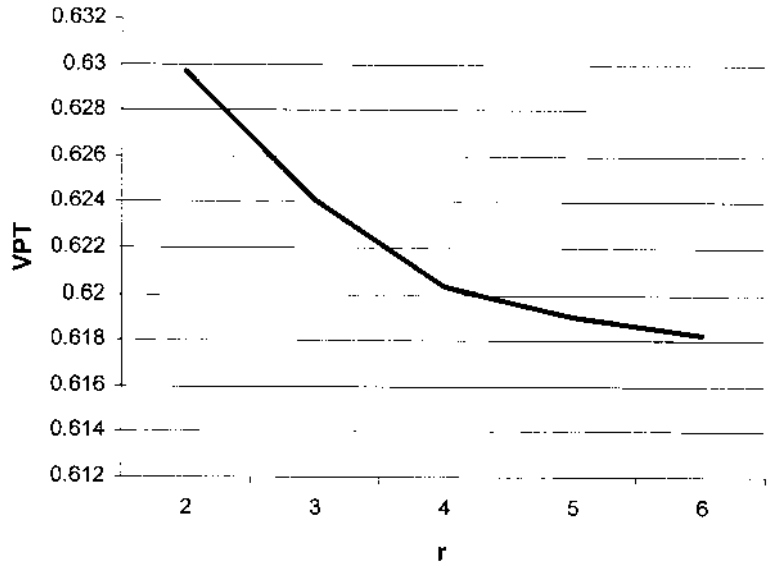

FIG. 4.20 Influence of the interior radius on VPT.

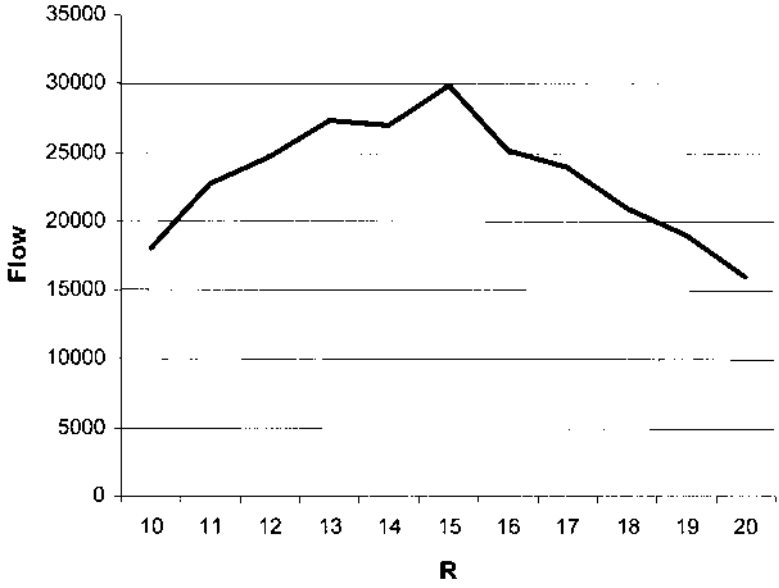

FIG. 4.21 Influence of the exterior radius on the total flow through the total exterior surface.

III. MECHANICAL PROPERTIES OF MICROPOROUS MATERIALS

A. Existing Theories of Mechanical Properties of Porous Solids

Existing theoretical methods for study of mechanical stability and resistance of materials are based on traditional theories of solid state. The employed approaches comprise

Statistical mechanics and thermodynamics [36–38]
Perturbation method [39,40]
Interface and colloid theory [41–43]
Phonon theory [44]
Cumulative damage theory [45]
Empirical models [46–48]

All these methods can be presented in analytical or numerical form. Some of them (e.g., Refs. 36–38, 41 and 42) are similar to the technique analyzed in Chapter 2. However, they do not account for the structural features of microporous materials. The fractal approach in the estimation of mechanical properties of solids was developed in Ref. 49.

In several cases, authors of models of mechanical properties of porous solids assume some geometry of microporous media. For example, Boccaccini et al. [43] elaborated a theoretical model for the prediction of Young's modulus of elasticity of porous materials, assuming a definite microstructural spheroidal model. The effective Young's modulus is given in Ref. 43 as a function of the volume fraction of closed porosity and the microstructural parameters: shape (axial ratio of the spheroidal pores) and orientation. According to Ref. 43, the microstructural parameters involved in the equation could be obtained from real microstructural data; then no fitting would be involved.

Since we already gave some criticisms of theories containing some assumptions of shape of micropores (see Chapters 1 and 3), we do not consider this model in detail.

As in the previous analysis, we find commendable to apply thermodynamics of nonequilibrium to the description of mechanical properties of porous materials. The principal advantages of thermodynamic approach to the solution of this problem consist in the following:

Thermodynamics allows taking into account the irreversibility of all processes related to deformations (if those are irreversible).
Thermodynamics considers all sequences of deformations as the motion of the treated system to a new thermodynamic equilibrium.

On the contrary to adsorption and permeability, mechanical properties of microporous structures are determined by all voids, comprising closed pores. This fact allows paying less attention to the microporous structure itself, and different solutions, particularly related to restructuring of porous media, become applicable.

B. Modeling of Mechanical Properties of Porous Solids, Using the Fractal Description

The fractal model of mechanical properties of solids is applicable to homogeneous randomly structured microporous materials. The fractal model assumes that the mechanical stability of solid structures is determined by elements of the continuous solid phase (fibers) [49]. The fiber substructure is considered as a fractal having dimensionality f_c. It is assumed that all fragments of the continuous solid phase (fibers) are fixed in the solid structure. Recall Chapter 1, we note that the considered material can be characterized, instead the pore distribution in energy or size, by an analogous distribution of fibers: energy distribution $F(E)$ or size distribution $\Phi(\rho)$, respectively.

From the considered material, a cubic sample is taken so carefully that the border effects can be neglected. The size of the sample is H; its volume is $V_0 = \mathrm{H}^3$. The sample is placed under a press performing pressure P on all sides. Because of the homogeneity of the sample, its deformation (h) is the same at all coordinates, and the mechanical resistance is characterized by the function $P(h)$. All changes in the sample are irreversible. At beginning of the process, $h = 0$, $P(h = 0) = 0$. The process is finished when all pores are destroyed: $h(\text{finish}) = h' = H\xi^{(1/3)}$, $P(h = h') = P'$, the pressure determined by the compressibility of the continuous solid phase. Every increase of the pressure causes destruction of several elements of the continuous solid phase. Such destruction depends on the thickness of these elements. Fiber having size ρ is destroyed into fractal cubes, each of which has dimensionality f_c and size ρ; such destruction needs energy:

$$E_d = Q_c \sigma_c \rho^{d_{fc}-1} \Phi(\rho) \tag{4.76}$$

where σ_c is the cohesion tension, Q_c is a normalizing coefficient, and d_{fc} is the fractal dimensionality of the fiber.

For the evaluation of mechanical stability and resistance of a microporous structure, the following subproblems need to be solved:

Correlation between different kinds of distribution functions found for the system

Thermodynamic functions of structural elements
Volume and energy balances regarding distribution functions

The process of formation of pores is related to the appearance of their walls belonging to fibers. The fibers form the continuous phase, the fractal with dimensionality f_c in a cubic initial volume $\omega_0 = h_0^3$, the porosity obtained is ξ_0, and the size of fiber is ρ. Such a system is described by the following equations:

$$\omega_p = \varsigma\omega_0 = r^{d_{f,p}} \tag{4.77}$$

$$\omega_c = (1 - \varsigma)\omega_0 = \rho^{d_{f,c}} \tag{4.78}$$

$$A_p = \varsigma_0 A_e + A_i = 2d_{f,p} r^{d_{f,p}-1} \tag{4.79}$$

$$A_c = (1 - \varsigma_0)A_e + A_i = 2d_{f,c}\ \rho^{d_{f,c}-1} \tag{4.80}$$

$$A_i = A_0\xi_0(1\ -\ \xi_0) \tag{4.81}$$

where A_0 is the initial total surface area, d_{fp} is the fractal dimensionality of porous cluster, A_i is the internal surface area, A_c and A_p are surface areas of the fiber and the pore, respectively, $A_e = 6h_0^2$ is the exterior surface area of the initial cube.

The combinatorial entropy of the continuous phase is found from:

$$\Delta S = R_g\omega_0[-\ln(\xi_0) - \ln(1 - \xi_0)] \tag{4.82}$$

The free energy of the continuous phase is

$$\Delta G_{cp} = \sigma_c A_e - T\Delta S \tag{4.83}$$

The chemical potential of the continuous solid phase is

$$\mu_{cp} = \Delta G_{cp}/V_{cp} \tag{4.84}$$

where V_{cp} is the volume of the continuous solid (fibers) phase.

Thus, we get a sequence of parameters available for evaluation: $\varepsilon - r - \rho$. Hence, knowing the function f(ε), we get all necessary forms of distributions.

1. Breaking-Up of Fibers

A fiber having characteristic size ρ has cohesive bond with the solid structure, the bond strength being $\sigma_c \rho^{(fc-1)}$. The volume of such fibers is proportional to their volume fraction $Q_c \Phi(\rho)\, d\rho$, while their number, respectively, is the same divided by the fiber volume: $Q_c \Phi(\rho)\, d\rho/\rho^{fc}$. Hence, the total strength of the cohesive bond of these fibers to the solid structure is $\sigma_c Q_c \Phi(\rho)\, d\rho/\rho$. The work performed by the exterior force destroying the fibers is found from

$$3P(h)(H-h)^2\, dh = Q_c \sigma_c \Phi(\rho)\, \frac{d\rho}{\rho} \tag{4.85}$$

On the other hand, the volume change is related to the reduction of the porous volume:

$$3(H-h)^2\, dh = q_p f(\varepsilon)\, d\varepsilon = Q_p \phi(r)\, dr \tag{4.86}$$

where ε and r are, respectively, the energy (per volume unit) and the size of the pores coexisting with the broken fibers and Q_p is a normalizing coefficient.

2. Size and Energy Distribution in the Continuous Solid Phase

In Chapter 3 we found the correlation between $f(\varepsilon)$ and the conditions of the preparation of microporous materials. Evaluations of other distributions (pores in size and fibers in energy and size) were not performed. However, it was shown in Ref. 50 that geometrical properties of porous and continuous phases are similar, and these substructures differ in the fractal dimensionality only. Considering them as cubes having different fractal dimensionalities (since fractals are not pores, we do not assume any shape of micropores), we may write the following equations:

$$V_p = \varsigma V_0 = L_p^{d_{f,p}} \tag{4.87}$$

$$V_c = (1-\varsigma) V_0 = L_c^{d_{f,c}} \tag{4.88}$$

$$A_p = 2d_{f,p} L_p^{d_{f,p}-1}, \qquad A_c = 2d_{f,c}\, L_c^{d_{f,c}-1} \tag{4.89}$$

where L_p and L_c are the formal linear sizes of the porous and continuous-solid clusters (fractals), respectively;

$$V_p = \int_{r_{\min}}^{r_{\max}} Q_p \phi(r)\, dr \tag{4.90}$$

$$V_c = \int_{R_{\min}}^{R_{\max}} Q_c \Phi(\rho)\, d\rho \tag{4.91}$$

$$U_p = \int_{r_{\min}}^{r_{\max}} Q_p \varepsilon(r) \phi(r)\, dr \tag{4.92}$$

$$U_c = \int_{R_{\min}}^{R_{\max}} Q_c E(\rho) \Phi(\rho)\, d\rho \tag{4.93}$$

On the other hand, the total pore volume and energy are found from the following equations, respectively,

$$V_p = \int_{\varepsilon_{\min}}^{\varepsilon_{\max}} q_e f(\varepsilon)\, d\varepsilon \tag{4.94}$$

$$U_p = \int_{\varepsilon_{\min}}^{\varepsilon_{\max}} q_e \varepsilon f(\varepsilon)\, d\varepsilon \tag{4.95}$$

There are two balances we can write for the system: those of volume and energy.

Volume balance is written as

$$dV = q_e f(\varepsilon)\, d\varepsilon \tag{4.96}$$

or:

$$dV = -Q_c \Phi(\rho)\, d\rho \tag{4.97}$$

where ρ is the size of a continuous solid substructure (fibers), q_e, Q_ρ is normalizing coefficients, and Φ is the function of distribution of fibers in size.

The energy balance of the system is given by

$$P(V)dV = Q_c \sigma_c \rho^{d_{f,c}-1} \Phi(\rho)\, d\rho \tag{4.98}$$

Equations (4.97) and (4.98) provide the correlation between V and P; hence, the system of equations (4.77)–(4.98) has the consistent solution and provides the information about such mechanical properties of the considered microporous system as mechanical stability and resistance.

Based on Eqs. (4.77)–(4.98), an example of calculations of mechanical resistance of a porous material vs. the deformation was presented in Ref. 49. It was found that the function resistance vs. deformation has a minimum. In the initial part of values of the arguments (high porosity) the resistance is high, due to the large fraction of micropores having small size, walls of which are not yet destroyed; in the end part of the values of the argument (very low porosity), the resistance rises sharply because there the fibers play much less important role than the resistance of the continuous phase entire (in which pores almost do not stay already).

C. Mechanical Properties of Polymers

The model presented above is applicable mostly to nonelastic porous solids, properties of which irreversibly change under an exterior tension loaded. That model is not valid for elastic microporous solids, first of all polymers, pore distribution in which may change because of the deformation caused by an exterior factor. Such a system is described by the statistical polymer method presented in Chapter 3.

1. Bonds in the Macromolecular Structure

The considered macromolecular system is characterized by the following interior bonds [51]:

Intermonomer bonds forming the macromolecules (not cross-linkage).
Cross-links: They influence the form and the characteristic size of macromolecules, in their energy of formation they are similar to intermonomer bonds, but their formation reduces the system entropy, and cross-links may get eventual tension because of the steric factor.
Weak intermacromolecular bonds: these form the structure from macromolecules.

Under an exterior pressure loaded, intermacromolecular bonds are destroyed first, this process being completely or partly irreversible. If the pressure loading is accompanied by heating, many cross-links are broken too, also this process is reversible. Intermonomer bonds and the rest of the cross-links (that eventually do not cause steric problems to their macromolecules) are destroyed under much higher pressures.

2. Structure of Macromolecular System

A macromolecular system with branching and without numerous cross-links may have a very high porosity. For several systems, that can be more 80% (e.g., silica gel [52]). If such a macromolecular mixture is treated under

pressure, there are found two factors reducing the porosity: additional cross-link formation and interpenetration of macromolecules. Interpenetration is understood as such a form of interactions of macromolecules that results in finding monomeric units belonging to a macromolecule inside the volume limited by monomeric units belonging to another macromolecule. The physical sense of interpenetration is the occupation of voids inside several macromolecules by other macromolecules.

The condition of additional cross-link formation is given by the equations derived in Chapter 3 for cross-linking, while interpenetration of two or more (μ) macromolecules is possible on condition that

$$\mu < M = \frac{1}{1-\xi} \tag{4.99}$$

where ξ is the maximal available local porosity (this corresponds to a system containing infinite macromolecules without cross-links or interpenetration); $\xi = (Z^3 - Z^{df})/Z^{df}$, where $Z(N)$ is the effective size of statistical N-mer. Equations for the evaluation of $Z(N)$ will be derived in Chapter 5, d_f is the fractal dimensionality of statistical N-mer.

A macromolecular system acted by an exterior pressure P is described by the following equation:

$$P\,dV_{mm} = dE_{mm} \tag{4.100}$$

where dV_{mm} and dE_{mm} are the changes of the volume and the interior energy of the macromolecular system, respectively:

$$dV_{mm} = dV_{cl} + dV_{ip} \tag{4.101}$$

$$dE_{mm} = dE_{cl} + dE_{ip} \tag{4.102}$$

where the terms with indices *cl* and *ip* mean cross-linking and interpenetration, respectively. For many of systems, the cross-linkage does not significantly depend on pressure, and the deformation is determined mostly by interpenetrations.

The whole volume of the macromolecular system can be divided into M zones containing (each) μ interpenetrating macromolecules. For the zones in which interpenetration is not found, we assume (by definition) $\mu = 1$, whereas the maximal available value of μ is M [see Eq. (4.99)]. The value of M is estimated by the statistical polymer method, as it is described above.

The system is characterized by distribution function $F(\mu)$ presenting the fraction of monomeric units found in zones of μ-times interpenetration. The amount of monomeric units, the volume, the energy, and the entropy are estimated from the following equations:

$$\nu_\Sigma \sim \sum_{\mu=1}^{M} F(\mu) \tag{4.103}$$

$$V_\Sigma \sim \sum_{\mu=1}^{M} \frac{F(\mu)}{\mu} \tag{4.104}$$

$$E_\Sigma = \sum_{\mu=1}^{M} \varepsilon_w \mu F(\mu) \tag{4.105}$$

$$S_\Sigma = -R_g \sum_{\mu=1}^{M} [F(\mu) \ln F(\mu)] \tag{4.106}$$

where ε_w is the energy of a single weak bond. Let us assume that the porosity of macromolecules does not directly depend on μ (meaning that the interpenetration does not change the form of macromolecules). For a system close equilibrium, the entropy is in a maximum, therefore little variations of left terms in Eqs. (4.103)–(4.106) give

$$\sum_{\mu=1}^{M} \delta F(\mu) = 0 \tag{4.107}$$

$$\sum_{\mu=1}^{M} \frac{\delta F(\mu)}{\mu} = 0 \tag{4.108}$$

$$\sum_{\mu=1}^{M} \mu \delta F(\mu) = 0 \tag{4.109}$$

$$\sum_{\mu=1}^{M} \delta F(\mu)[\ln F(\mu) + 1] = 0 \tag{4.110}$$

From Eqs. (4.108)–(4.110) we obtain

$$\sum_{\mu=1}^{M} \delta F(\mu)\left[\ln F(\mu) + \gamma_1 + \mu\gamma_2 + \gamma_3/\mu\right] = 0 \tag{4.111}$$

where γ_1, γ_2, γ_3 are some coefficients. Eq. (4.111) can be rewritten, taking into account that these coefficients are related to the parameters of interpenetration:

$$F(\mu) = A_F \exp\left[\frac{\beta_\nu}{\mu} + \beta_e \varepsilon_w \mu\right] \tag{4.112}$$

Equations (4.108)–(4.112) provide the complete description of a macromolecular structure with interpenetration, while other effects (e.g., cross-linking) should be accounted for separately.

If interpenetration is accompanied by cross-linking, the contribution of each process to the total mechanical resistance is estimated from the following equations for volume, energy, and entropy:

$$\delta V_\Sigma = \delta V_{ip} + \delta V_{cl} \tag{4.113}$$

$$\delta E_\Sigma = \delta E_{ip} + \delta E_{cl} \tag{4.114}$$

$$\delta S_\Sigma = \delta S_{ip} + \delta S_{cl} = \text{maximum} \Longrightarrow \delta S_{ip} = \delta S_{cl} \tag{4.115}$$

Let us notice that the mechanical equilibrium for branched macromolecules is related to several cross-linking and interpenetration. When we talk about the interpenetration and cross-linking mechanisms for the deformation, we mean ''additional'' cross-linking or/and interpenetration. For deformations caused by compression (the current volume below the equilibrium volume), the number of cross-links is more than in equilibrium, while for decompression (the current volume above the equilibrium volume), the situation is contrary (reduction of the number of cross-links). The tendency to interpenetration, respectively, predominates under the compression, while decompression decreases the factor of interpenetration.

The above equations allow us to estimate mechanical characteristics of macromolecular systems. For example Fig. 4.22 presents the value of pressure needed for cross-linking of different macromolecules.

As follows from Fig. 4.22, the most contribution to the mechanical resistance of polymeric materials is due to low-degree macromolecules. Since cross-linking is a high-energy process (on the contrary to interpenetration, which is a low-energy process, as noted above), cross-linking takes place mostly under lower pressures. The pressure needed for the formation of one additional cross-link in a macromolecule depends much on its weight: the increase of the degree of polymerization leads to the reduction of the pressure needed. This result is in accordance with known facts, such as the steric difficulties for the formation of cross-link in short macromolecules.

Now, let us consider the aspect of the relationship between interpenetration and the needed pressure. Figure 4.23 presents the value of pressure needed for interpenetration of macromolecules.

As follows from Fig. 4.23, the contribution of interpenetration increases with the deformation. The curve pressure vs. deformation exhibits a slow increase of the derivative. Physically, that means that the interpenetration is nonlinear factor of deformation.

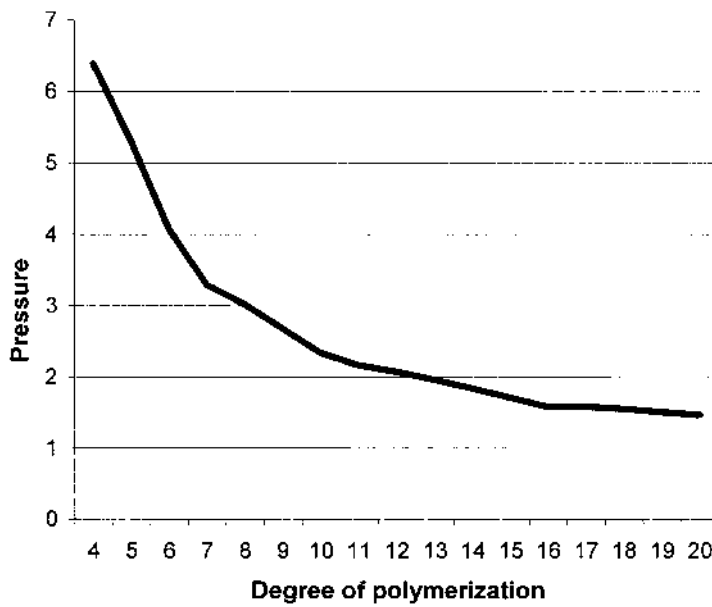

FIG. 4.22 Pressure needed for additional cross-linking in macromolecules (number of branching $m = 5$).

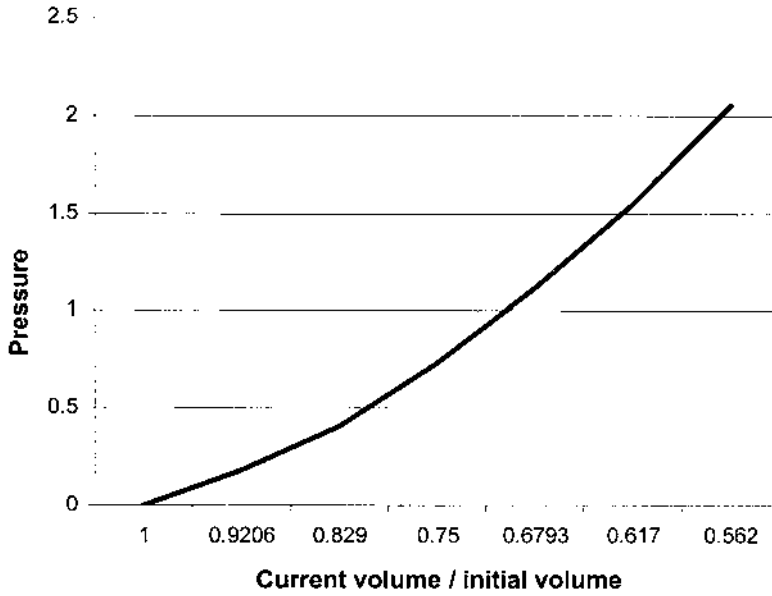

FIG. 4.23 Pressure needed for interpenetration of macromolecules.

We notify that all kinds of deformations of polymeric materials can be considered as declinations of cross-linkage and interpenetration from their equilibrium values.

IV. CONCLUSIONS

1. A principal problem in the preparation and the uses of adsorbents consists in the difficulties in avoiding the adsorption of undesirable fluids. In real industrial conditions, freshly prepared adsorbents may contain undesirable volatile components that reduce the adsorptive effectiveness of industrial adsorbents and may cause wrong results of experiments with the adsorbents.
2. The principal drawbacks of the existing volume-filling micropore theory (VFMT), assuming that adsorption in micropores is limited by their volume, include
   a. The condensation approximation assuming that filling of micropores is determined only by their energy
   b. Baseless assumptions about the energy distribution of micropores

3. The recently proposed Langmuir-like theory of filling of micropores, based on the assumption of Langmuir-like mechanism of pore–adsorbate interactions, neutralizes both above disadvantages of VFMT.
4. Both VFMT and Langmuir-like models suggest adsorption isotherm curves, the form of which is in accordance with experimental data. However, fitted parameters appearing in the Langmuir-like model are not empirical but semiempirical, on the contrary to VFMT. These parameters are more sensitive to properties of adsorbate. In the case of heterogeneous structures, the advantages of the Langmuir-like model become even more significant, because this does not need additional fitted parameters for taking into account the factor of heterogeneity (on the contrary to VFMT).
5. Among the existing models of percolation and permeability, the random trajectory approach is definitely preferable (for modeling both percolation and permeability), due to its ability to bring the relationship between the microscopic characteristics of a porous structure (distribution of solid particles in the number of their near neighbors) and its measurable properties.
6. The random trajectory method allows the solution of practically important problems, such as the evaluation of the permeability of catalyst carrier (in the simulation of mass transfer in the heterogeneous catalysis). All principal results obtained in the random trajectory model of catalyst carrier are in the accordance with known experimental facts.
7. Among existing theories of mechanical properties of porous materials, the following thermodynamic approaches are preferable:
   a. The fractal-based model of irreversible changes in porous material acted by exterior tension
   b. The statistical polymer-based model of reversible changes in polymeric porous material under exterior tension

REFERENCES

1. Gregg, S.J.; Sing, K.S.W. *Adsorption*, *Surface Area*, *and Porosity*. 2nd ed.; Academic Press: London, 1982.
2. Noll, K.E.; Gounaris, V.; Hou, W.-S. *Adsorption Technology* (*For Air and Water Pollution Control*); Lewis Publishers: Chelsea, 1991.
3. Rudzinski, W.; Everett, D.H. *Adsorption of Gases on Heterogeneous Surfaces*; Academic Press: London, 1992.

4. Heffelfinger, G.S.; Van Swol, F.; Gubbins, K.E. Adsorption hysteresis in narrow pores. J. Chem. Phys. **1988**, *89* (8), 5202–5205.
5. Bojan, M.J.; Van Slooten, R.; Steele, W. Computer simulation studies of the storage of methane in microporous carbons. Sep. Sci. Technol. **1992**, *27* (14), 1837–1856.
6. Visscher, P.B.; Cates, J.E. Simulation of porosity reduction in random structures. J. Mat. Res. **1990**, *5* (10), 2184–2196.
7. Dubinin, M.M. Physical feasibility of Brunauer's micropore analysis method. J. Coll. Interface Sci. **1974**, *46* (3), 351–356.
8. Dubinin, M.M.; Astakhov, V.A. Development of theories on the volume filling of micropores during the adsorption of gases and vapors by microporous adsorbents. 1. Carbon adsorbents. Izvestiya Akademii Nauk SSSR, Seriya Khimicheskaya **1971**, (1), 5–11.
9. Stoeckli, F.; Morel, D. On the physical meaning of parameters E0 and β in Dubinin's theory. Chimia **1980**, *34* (12), 502–503.
10. Huber, U.; Stoeckli, F.; Houriet, J.P. A generalization of the Dubinin–Radushkevich equation for the filling of heterogeneous micropore systems in strongly activated carbons. J. Coll. Interface Sci. **1978**, *67* (2), 195–203.
11. Stoeckli, F.; Ballerini, L. Evolution of microporosity during activation of carbon. Fuel **1991**, *70* (4), 557–559.
12. McEnaney, B. Estimation of the dimensions of micropores in active carbons using the Dubinin–Raduskevich equation. Carbon **1987**, *25* (1), 69–75.
13. Stoeckli, H.F.; Houriet, J. Ph. The Dubinin theory of micropore filling and the adsorption of simple molecules by active carbons over a large range of temperature. Carbon **1976**, *14* (5), 253–256.
14. Romm, F. Thermodynamic description of a microporous material formation (linear steady-state approximation). J. Coll. Interface Sci. **1996**, *179* (1), 1–11.
15. Tsunoda, R. Determination of micropore volumes of active carbon using Dubinin–Radushkevich plots. Bul. Chem. Soc. Japan **1977**, *50* (8), 2058–2062.
16. Tsunoda, R. Adsorption of water vapor on active carbons: estimation of pore width. J. Coll. Interface Sci. **1990**, *137* (2), 563–570.
17. Tsunoda, R. Relationships between adsorption parameters of the BET and the Dubinin–Radushkevich equations in nitrogen adsorption on active carbons. J. Coll. Interface Sci. **1987**, *117* (1), 291–292.
18. Romm, F. Thermodynamics of microporous material formation. In: *Surfactant Science Series*, *Interfacial Forces and Fields: Theory and Applications* (Monographic series, ed.: Hsu, J.-P.), Chapter 2; Marcel Dekker: New York, 1999, pp. 35–80.
19. Romm, F. Thermodynamic description of formation of a microporous material (non-steady-state approximation). J. Coll. Interface Sci. **1996**, *179* (1), 12–19.
20. Romm, F. Derivation of the equations for isotherm curves of adsorption on microporous gel materials. Langmuir **1996**, *12* (14), 3490–3497.
21. Rudzinski, W.; Steele, W.A.; Zgrablich, G. Equilibria and dynamics of gas adsorption on heterogeneous solid surfaces. *Stud Surf. Sci. Catal.*, 1997; 104. Elsevier: Amsterdam, Neth., 1997.

22. Pride, S.R.; Flekkoy, E.G. Two-phase flow through porous media in the fixed-contact-line regime. Geosciences Rennes, Universite de Rennes 1, Rennes, Fr. Phys. Rev. E: Statistical Physics, Plasmas, Fluids, and Related Interdisciplinary Topics **1999**, *60* (4-B), 4285–4299.
23. Kling, A.; Barao, F.; Nakagawa, M.; Tavora, L.; Vaz, P. (Eds.). *Advanced Monte Carlo for Radiation Physics, Particle Transports Simulation and Applications*. Proc. Conf. 2000, Lisbon, Portugal, 2001.
24. Cohen, R.; ben-Avraham, D.; Havlin, S. Percolation critical exponents in scale-free networks. Phys. Rev. E: Statistical, Nonlinear, and Soft Matter Physics **2002**, *66* (3-2A), 36113/1–36113/4.
25. Davies, Graham M.; Seaton, Nigel A. Predicting adsorption equilibrium using molecular simulation. AIChE J. **2000**, *46* (9), 1753–1768.
26. Heuchel, M.; Davies, G. M.; Buss, E.; Seaton, N. A. Adsorption of carbon dioxide and methane and their mixtures on an activated carbon: Simulation and experiment. Langmuir **1999**, *15* (25), 8695–8705.
27. Murray, K.L.; Seaton, N.A.; Day, M.A. Use of mercury intrusion data, combined with nitrogen adsorption measurements, as a probe of pore network connectivity. Langmuir **1999**, *15* (23), 8155–8160.
28. Davies, G.M.; Seaton, N.A. The effect of the choice of pore model on the characterization of the internal structure of microporous carbons using pore size distributions. Carbon **1998**, *36* (10), 1473–1490.
29. Boulton, K. L.; Lopez-Ramon, M. V.; Davies, G. M.; Seaton, N. A. Effect of assumed pore shape and interaction parameters on obtaining pore size distributions from adsorption measurements. Special Publication—Royal Society of Chemistry 1997, *213*(Characterisation of Porous Solids IV), 504–511.
30. Lopez-Ramon, M.V.; Jagiello, J.; Bandosz, T.J.; Seaton, N.A. Determination of the Pore Size Distribution and Network Connectivity in Microporous Solids by Adsorption Measurements and Monte Carlo Simulation. Langmuir **1997**, *13* (16), 4435–4445.
31. Schoelkopf, J.; Ridgway, C.J.; Gane, P.A.C.; Matthews, G.P.; Spielmann, D.C. Measurement and network modeling of liquid permeation into compacted mineral blocks. J. Coll. Interface Sci. **2000**, *227* (1), 119–131.
32. Gane, P.A.; Kettle, J.P.; Matthews, G.P.; Ridgway, C.J. Void space structure of compressible polymer spheres and consolidated calcium carbonate paper-coating formulations. Ind. Engng. Chem. Res. **1996**, *35* (5), 1753–1764.
33. Romm, F. Modeling of percolation–permeability in microporous systems. J. Coll. Interface Sci. **2000**, *232* (1), 121–125.
34. Romm, F. Random Trajectory Modeling of limited-volume percolation in a microporous structure. J. Coll. Interface Sci. **2001**, *240* (1), 368–371.
35. Romm, F. Evaluation of permeability of microporous media, using the modified random-trajectory approach. J. Coll. Interface Sci. **2002**, *250* (1), 191–195.
36. Kikuchi, R.; Chen, L.-Q. Theoretical investigation of the thermodynamic stability of nanoscale systems III. Thin film with an IPB. Nanostruct. Mat. **1995**, *5* (7/8), 745–754.

37. Henderson, J. R. Potential-distribution theorem. Mechanical stability and Kirkwood's integral equation. Mol. Phys. **1983**, *48* (4), 715–717.
38. Bessenrodt, R.; Schnittker, P. Applications of a nonlinear stability theory for the stationary states of isothermal networks. Zeitschrift fuer Physik **1974**, *268* (2), 217–224.
39. Blasbalg, D.A.; Salant, R.F. Numerical study of two-phase mechanical seal stability. Tribology Transactions **1995**, *38* (4), 791–800.
40. Reiser, B. On the lattice stability of metals. II. Two perturbation formalisms for the comparison of crystals with different lattices. Theoret. Chim. Acta **1976**, *43* (1), 37–43.
41. Mastrangelo, C.H.; Hsu, C.H. Mechanical stability and adhesion of microstructures under capillary forces. Part I: Basic theory. J. Microelectromech. Sys. **1993**, *2* (1), 33–43.
42. Pendle, T.D.; Gorton, A.D.T. The mechanical stability of natural rubber latexes. Rub. Chem. Technol. **1978**, *51* (5), 986–1005.
43. Boccaccini, A.R.; Ondracek, G.; Postel, O. Young's modulus of porous ceramics. Silic. Indus. **1994**, *59* (9–10), 295–299.
44. Moleko, L.K.; Glyde, H.R. Vibrational stability and melting. Phys. Rev. B: Condensed Matter and Materials Physics **1983**, *27* (10), 6019–6030.
45. Tateishi, T. Continuum theory of cumulative damage. Bull. JSME **1976**, *19* (135), 1007–1018.
46. Polyakov, V.V.; Golovin, A.V. Elastic characteristics of porous materials. Prikladnaya Mekhanika i Tekhnicheskaya Fizika **1993**, (5), 32–35.
47. Cooper, R. E.; Rowland, W.D.; Beasley, D. Survey of the effects of porosity on the elastic moduli and strength of brittle materials with particular reference to beryllium. U.K. At. Energy Auth., At. Weapons Res. Estab., Rep. **1971**, AWRE O *25*/71.
48. Ferrari, F.; Rossi, S.; Bonferoni, M. C.; Caramella, C. Rheological and mechanical properties of pharmaceutical gels. Part I: Nonmedicated systems. Boll. Chim. Farm. **2001**, *140* (5), 329–336.
49. Romm, F.; Figovsky, O. Estimation of mechanical stability and resistance of microporous materials prepared by pyrolysis. J. Solid State Chem. **2001**, *160* (1), 13–16.
50. Romm, F. Modeling of the internal structure of randomly formed microporous material of unlimited volume, following thermodynamic limitations. J. Coll. Interface Sci. **2000**, *227* (2), 525–530.
51. Romm, F.; Figovsky, L. Theoretical modeling of mechanical resistance and stability and related characteristics of polymeric systems with branching/cross-linking. J. Solid State Chem. **2002**, *164* (2), 237–245.
52. Iler, R.K. *The Chemistry of Silica* : *Solubility, Polymerization, Colloid and Surface Properties*, *and Biochemistry*. Wiley-Interscience: New York, 1979.